Geoscientific
Model Development

Air quality forecasts on a kilometer-scale grid over complex Spanish terrains

M. T. Pay[1,*], **F. Martínez**[1], **M. Guevara**[1], **and J. M. Baldasano**[1,2]

[1]Earth Sciences Department, Barcelona Supercomputing Center-Centro Nacional de Supercomputación, Barcelona, Spain
[2]Environmental Modeling Laboratory, Technical University of Catalonia, Barcelona, Spain
[*]now at: Laboratoire de Météorologie Dynamique, École Polytechnique, Palaiseau, France

Correspondence to: M. T. Pay (maria.pay@bsc.es)

Abstract. The CALIOPE Air Quality Forecast System (CALIOPE-AQFS) represents the current state of the art in air quality forecasting systems of high-resolution running on high-performance computing platforms. It provides a 48 h forecast of NO_2, O_3, SO_2, PM_{10}, $PM_{2.5}$, CO, and C_6H_6 at a 4 km horizontal resolution over all of Spain, and at a 1 km horizontal resolution over the most populated areas in Spain with complex terrains (the Barcelona (BCN), Madrid (MAD) and Andalusia (AND) domains). Increased horizontal resolution from 4 to 1 km over the aforementioned domains leads to finer textures and more realistic concentration maps, which is justified by the increase in NO_2 / O_3 spatial correlation coefficients from 0.79/0.69 (4 km) to 0.81/0.73 (1 km). High-resolution emissions using the bottom-up HER-MESv2.0 model are essential for improving model performance when increasing resolution on an urban scale, but it is still insufficient. Decreasing grid spacing does not reveal the expected improvement in hourly statistics, i.e., decreasing NO_2 bias by only $\sim 2\,\mu g\,m^{-3}$ and increasing O_3 bias by $\sim 1\,\mu g\,m^{-3}$. The grid effect is less pronounced for PM_{10}, because part of its mass consists of secondary aerosols, which are less affected than the locally emitted primary components by a decreasing grid size. The resolution increase has the highest impact over Barcelona, where air flow is controlled mainly by mesoscale phenomena and a lower planetary boundary layer (PBL). Despite the merits and potential uses of the 1-km simulation, the limitations of current model formulations do not allow confirmation of their expected superiority close to highly urbanized areas and large emissions sources. Future work should combine high grid resolutions with techniques that decrease subgrid variability (e.g., stochastic field methods), and also include models that consider urban morphology and thermal parameters.

1 Introduction

The World Health Organization (WHO) has recently shown that there is sufficient evidence that particulate matter (PM), ozone (O_3) and nitrogen dioxide (NO_2) affect human health (WHO, 2013). Although NO_2 and PM concentrations improved from 2002 to 2011 in Europe, the situation is still far from matching the WHO air quality guidelines (AQG). The European annual limit values for NO_2 (annual) and PM_{10} (daily) had been exceeded at 42–43 % of the traffic stations in 2011. For the same year, about 33 % of the European urban population was exposed to PM_{10} concentrations above the daily limit value, and nearly 88 % was exposed to the respective WHO AQG (EEA, 2013). Air pollution legislation for the protection of the increasing city population has recently increased the demand for forecasting systems that can assess and understand air pollution dynamics, alert the population when health-related issues occur, and develop emission abatement plans (EEA, 2011).

When applying an air quality modeling system, defining the grid resolution is an important consideration. The potential benefits of higher-resolution modeling should be weighed against the increased complexity of the inputs, increased CPU time, and disk space requirements. In theory, higher-resolution modeling is expected to yield more accurate forecasts because of better resolved model input fields (topography, land cover and emissions). Furthermore, high resolutions (ranging from 1 to 5 km) are essential for reproducing mesoscale phenomena, e.g., those controlling O_3 transport along the mountainous northeastern Mediterranean coast (Fay and Neunhäuserer, 2006; Jiménez et al., 2006). Even on fine scales, the modeled concentrations are not necessarily the best (Mass et al., 2002; Gego et al., 2005; Valari

and Menut, 2008), because increasing emission and meteorology spatial resolution can also increase uncertainties, at the risk of reduced model performance. Nowadays, fine horizontal resolution is a persistent challenge when assessing health impacts and population exposure studies (Thompson et al., 2014).

Several studies have evaluated the impact of increasing horizontal resolution on different scales over the eastern and southeastern USA using the Community Multiscale Air Quality (CMAQ) model and the Comprehensive Air Quality Model with Extensions (CAMx), which range from 32 to 12 to 4 km (Cohan et al., 2006; Tesche et al., 2006; Queen and Zhang, 2008). They found no significant changes for O_3 and PM ($< 5\%$ on average), and those changes were even smaller at resolutions of between 12 and 4 km ($< 3\%$). Concerning PM components, Fountoukis et al. (2013) found that increased resolution provides differences mostly for primary PM rather than for secondary PM. Recently, a model intercomparison exercise, named ScaleDep, was performed to determine the effect of grid resolution on air quality modeling performance over Europe on a regional and urban scale (Cuvelier et al., 2013). The exercise, involving five chemical transport models (CTMs) (EMEP, CHIMERE, CMAQ, LOTOS-EUROS and RCGC) running under the same conditions over the full year of 2009 and at four resolutions (56, 28, 14, and 7 km), showed that it is difficult to define a grid size that is adequate for resolving the urban signal under all conditions affecting Europe. Still, a 14-km resolution seems to be a good compromise between background applications and those reproducing most of the urban signals (7-km resolution). However, the ScaleDep exercise did not distinguish between the different topographies or complex meteorological patterns that are characteristic of the Iberian Peninsula.

Few studies have been performed over selected areas in Spain, and of those, the focus has been mainly on O_3 and NO_2. Vivanco et al. (2008) evaluated the annual impact by increasing the model resolution (to 36, 19, and 7 km) over Madrid for NO_2 and O_3. They used the WRF-CHIMERE model, disaggregating the EMEP emissions inventory based on land-use information. Their evaluation showed that the model improved more for NO_2 than O_3, with the most significant improvement achieved when the resolution increases from 36 to 19 km rather than to 7 km, which they linked to increased uncertainty in the emissions data introduced with the disaggregation techniques. Jiménez et al. (2006) used the MM5-CMAQ model along with a bottom-up emissions model EMICAT2000, Air Pollutants Emission from Catalonia during the year 2000 to assess the influence of grid resolution on O_3 (at 8, 4, and 2 km) over the complex terrain of the northeastern Iberian Peninsula (Catalonia) during a summer pollution episode. They found that both an improved performance of the mesoscale phenomena and a better allocation of emissions for the 2-km resolution improve the capability of the model to simulate exceedances of European limit values. An important issue in both studies is the emissions

modeling approach (top-down vs. bottom-up) when applying high resolutions on a local scale (< 10 km). As Fountoukis et al. (2013) and Timmermans et al. (2013) demonstrate, in the range of local scales (e.g., the greater Paris area), the grid resolution is not currently the major source of discrepancies in model performance, but instead the predicted concentrations and corresponding gradients are more consistent with observed concentrations when provided by bottom-up emissions inventories rather than by downscaled inventories. If local variation in input data (e.g., emissions patterns or land use) cannot be characterized properly, modeling with a finer grid resolution may not provide any great advantages.

Increasing resolution is a technical challenge, since computational cost markedly increases in inverse proportion to grid spacing. The current progress in computation allows increased model resolution and for multiple spatial scales to be investigated, with the aim of establishing an adequate grid size for forecasting air quality on the local scale. Recently, Colette et al. (2014) evaluated the impact of increasing resolution up to 2 km over the European continent by using the CHIMERE model for an episode of air pollution in 2009. They simulated 2 million grid cells using over 2000 CPUs of a high-performance computing system, which was hosted by the French Computing Centre for Research and Technology (CCRT/CEA).

In terms of computational resources, horizontal resolution is critical to an operational air quality forecast. In Europe, operational air quality systems use resolutions between 12 and 25 km, while applications to a single country can reach resolutions between 4 and 10 km (Zhang et al., 2012). Over Spain, there are three systems providing air quality forecasts running at different horizontal resolutions. The lowest resolution system is the Technical University of Madrid's OPANA (OPerational Atmospheric Numerical model for urban and regional Areas), running at 27 km $\times$ 27 km and based on the MM5/CMAQ/EMIMO models (San José et al., 2009). It is followed by the Spanish meteorological office's system (AEMET, http://www.aemet.es/es/eltiempo/prediccion/calidad_del_aire), which forecasts at 10 km $\times$ 10 km using the HIRLAM-HNR/MOCAGE/GEMS-TNO models. The CALIOPE Air Quality Forecast System (CALIOPE-AQFS; Baldasano et al., 2011; Pay et al., 2012a, and references therein), of the Barcelona Supercomputing Center–Centro Nacional de Supercomputación (BSC-CNS), runs at the highest resolution, 4 km $\times$ 4 km, and it is based on the WRFv3.5/CMAQv5.0.1/HERMESv2.0/BSC-DREAM8bv2 models. Moreover, CALIOPE-AQFS provides 1 km $\times$ 1 km resolution forecasts for the Madrid and Barcelona metropolitan areas (since 2009) and the Andalusian region (since 2013). Such a resolution has been possible thanks to both the high-performance computing resources at the BSC-CNS and the availability of detailed emissions data covering Spain.
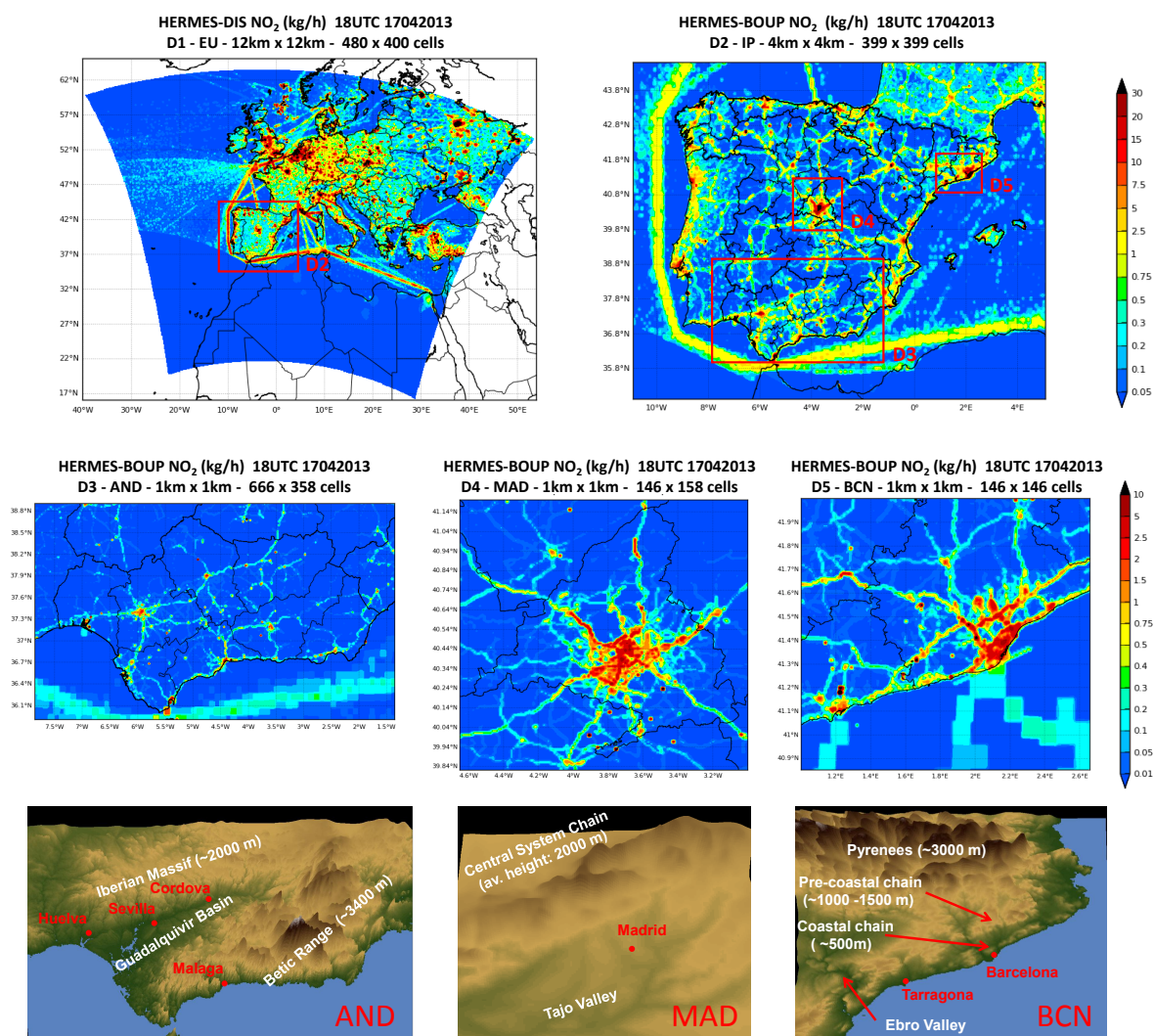
Figure 1. CALIOPE-AQFS nesting strategy (D domains) and study domains (Andalucia, AND; Madrid, MAD; and Barcelona, BCN). The color chart at the D domains shows the NO_2 emission rate ($kg\,h^{-1}$) for 17 April 2013 at 18:00 UTC. The HERMESv2.0 model generates emissions at $12\,km \times 12\,km$ over Europe (the mother domain, D1) by performing disaggregation from the EMEP database. The HERMESv2.0 model estimates emissions at $1\,km \times 1\,km$, following a bottom-up approach.

The present work aims to assess the impact of increasing the horizontal resolution from 4 to 1 km, specifically over areas affected by heterogeneous emission patterns and complex terrains such as the Barcelona and Madrid metropolitan areas (BCN and MAD), together with the Andalusian region (AND). For that purpose, the CALIOPE-AQFS forecasts pollutant concentrations (O_3, NO_2, and PM_{10}) at two horizontal resolutions: first at a 4-km resolution covering Spain (IP4), and second at a 1-km resolution covering the AND, BCN, and MAD domains. Here, a study is performed for the period April 2013, which presents a 7-day air pollution episode. We use observations from routine air quality monitoring networks to evaluate both resolutions.

Section 2 describes the configuration and computational setup of CALIOPE-AQFS. Section 3 quantifies the impact of resolution increase on forecasting hourly concentrations (and exceedances) in terms of pollutant, domain, building density and major emission sources. Section 4 concludes with the main results and some recommendations.

2   Methodology

2.1   Domain and period under study

Figure 1 shows the primary NO_2 emission patterns and topographic characteristics of the BCN, MAD and AND domains. BCN is a coastal area characterized by several valleys perpendicular to the coastline and two main mountain

ranges, one coastal (500 m in height) and one pre-coastal (1000–1700 m in height). These features induce mesoscale phenomena such as sea-breeze and mountain-valley winds. On the other hand, MAD is a continental region with a much simpler topography that includes the Tajo Valley in the south and the mountain range of the Central System in the north, with summits reaching 2500 m.

The urban contribution in BCN (3.1 million inhabitants) is accompanied by industrial and power generation emissions, the road network and the harbor. Meanwhile, the Spanish capital of MAD is mainly influenced by emissions from the urban area (5.8 million inhabitants) and the road network that connects MAD with the surrounding commercial and industrial zones, as well as the urban areas.

AND is the southernmost region in Spain, with complex topography characterized by the large depression of the Guadalquivir Basin (delimited by the Iberian Massif and the Betic Range), which crosses the region from NE to SW over a 60 km stretch. About three quarters of AND has a mountainous orography, including the Sierra Nevada (3481 m). AND includes one of the five biggest cities in Spain, Seville (∼ 700 000 inhabitants), which hosts industrial and electric generation activities around the Algeciras bay, and is affected by dense maritime traffic through the Strait of Gibraltar.

The study is done for April 2013. At the beginning and end of the month, the synoptic circulation was controlled by a low-pressure system located over the south of the British Isles, and affected Western Europe by leading to atmospheric instability over the IP. This pattern is typical of transitional months such as April and November (García-Valero et al., 2012; Valverde et al., 2014), which produce precipitation and low temperatures because of cold and humid winds from the Atlantic Ocean. In contrast, from 12 to 18 April, there was a high pressure system crossing the Iberian Peninsula in the SW–NE direction, transporting dust from the Sahara Desert and increased temperatures up to 25–28 °C, confirmed by the mineral dust forecasts of the BSC-DREAM8b model (http://www.bsc.es/earth-sciences/mineral-dust-forecast-system/bsc-dream8b-forecast). During the latter episode, available air quality stations in the study domains observed several exceedances of the European limit values (8 exceedances of the NO_2 hourly limit value, 25 exceedances of the O_3 information threshold, and 31 exceedances of the PM_{10} daily limit value).

2.2 CALIOPE-AQFS

CALIOPE-AQFS has provided 48 h air quality forecasts for Europe and Spain since October 2006 (www.bsc.es/caliope), and has been described and evaluated in detail elsewhere (Baldasano et al., 2008, 2011; Pay et al., 2011, 2012a). Briefly, it integrates a meteorological model (WRF-ARW v3.5; Skamarock and Klemp, 2008), an emissions model (HERMESv2.0; Guevara et al., 2013), a chemical transport model (CMAQv5.0.1; Byun and Schere, 2006; Appel

et al., 2013), and a mineral dust atmospheric model (BSC-DREAM8bv2; Pérez et al., 2006; Basart et al., 2012); together, all of these comprise an air quality forecast system.

Figure 1 shows the working domains of the CALIOPE-AQFS. First, CALIOPE-AQFS was run over Europe at a 12 km × 12 km horizontal resolution using initial/boundary conditions from the final analyses of the National Centers of Environmental Prediction (FNL/NCEP). The analyses began at 12:00 UTC, at intervals of 6 h (0.5° × 0.5°) for meteorology. The LMDz-INCA2 global model (3.75° × 2.5°; Szopa et al., 2009) was used for chemistry. Then, CALIOPE-AQFS was run at 4 km × 4 km horizontal resolution (IP4) over the IP using one-way nesting. In the present work CALIOPE-AQFS runs at 1 km × 1 km over the AND, BCN and MAD domains, with a nesting of over the IP4 domain. HERMESv2.0 forecasts anthropogenic emissions for the year 2009 by following a bottom-up methodology (point, linear and area), and biogenic emissions using the MEGANv2.0.4 model (Guenther et al., 2006). Emissions are aggregated into 1 km grids for the AND, BCN and MAD 1 km simulations, and into a 4 km grid for IP4.

Vertically, WRF-ARW is configured with 38 sigma layers up to 50 hPa, with 11 characterizing the planetary boundary layer (PBL). Meanwhile, the CMAQ vertical levels are obtained by collapsing from the 38 WRF levels to a total of 15 layers whose depth increases with height, from the surface up to 50 hPa. Six layers are within the PBL, and the first layer depth is 39 m.

The present WRF setup uses the rapid radiation transfer model (RRTM) and Dudhia for long- and short-wave radiation, respectively, the Kain–Fritsch cumulus parameterization (Kain and Fritsch, 1990), the single-moment 3-class (WSM3) microphysics scheme, and the Yonsei University PBL scheme (YSU). The Noah land-surface model (NoahLSM), based on the US Geological Survey (USGS) land-use data from the year 1993, is used by default in the present WRF configuration.

Currently, a new CMAQ version is being tested in the Community Modeling and Analysis System (CMAS) community, namely CMAQv5.0 (CMAQ, 2014). It includes substantial scientific improvements over version 4.5, and is especially devoted to improving secondary organic aerosol (SOA) formation as well as the dynamic interactions of fine and coarse aerosols. Based on the evaluation results from the previous CMAQ version within CALIOPE-AQFS (4.5 vs. 5.0) (Pay et al., 2012b), CMAQ has been updated to version 5.0.1 using the CB05 chemical mechanism (Yarwood et al., 2005), the AERO5 for aerosol modeling, and the in-line photolysis calculation. Although not used here, future simulations will use the updated version of the aerosol module (AERO6), which includes a significant improvement in the science of the primary organic aerosol aging and the sulfur chemistry.

CALIOPE-AQFS considers desert dust contribution by means of the BSC-DREAM8bv2, which runs offline at a 0.5° × 0.5° resolution covering Europe, North Africa and
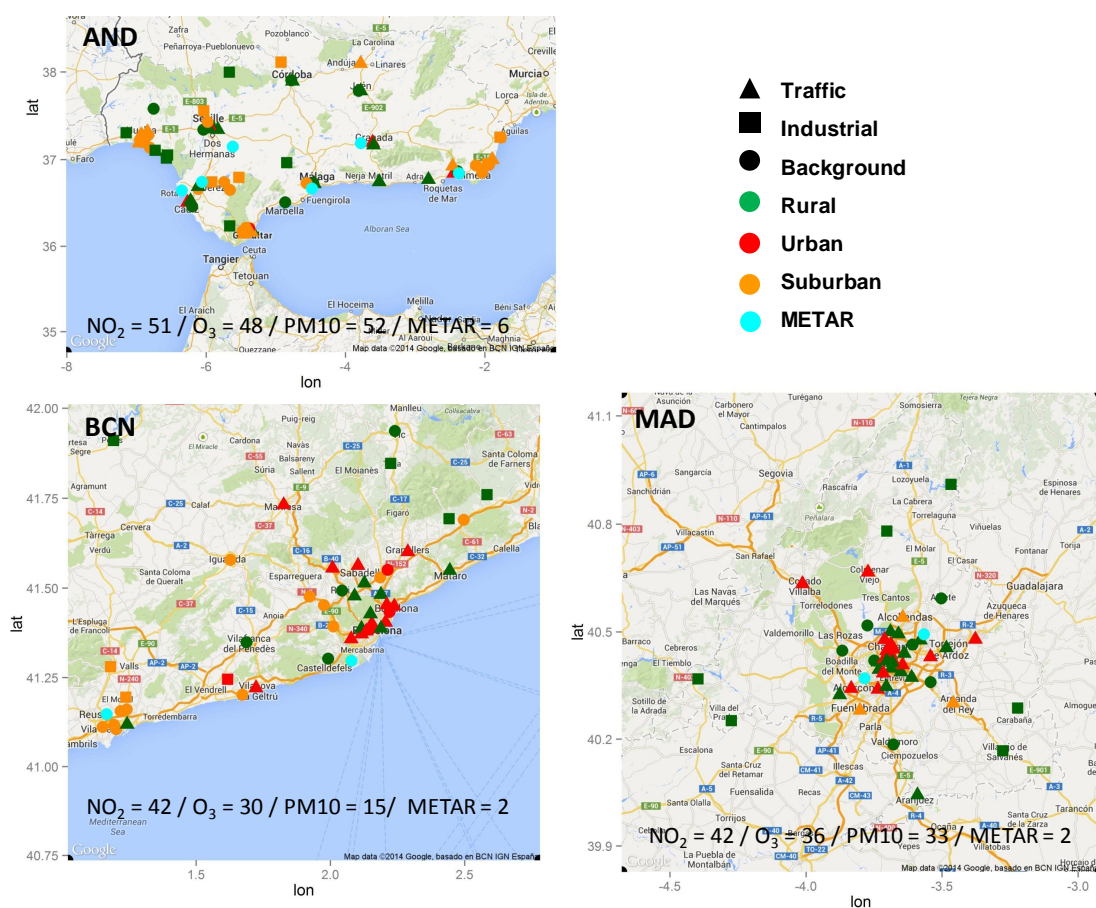
Figure 2. Air quality stations for NO_2, O_3 and PM_{10} in the three domains under study (AND, BCN and MAD) in April 2013. Different types of stations are shown by symbols and color codes. The various symbols represent the major emission type affecting each station (Traffic: triangle; Industrial: square; and Background: circle), while the colors reflect the environment of each station (Urban: red; Suburban: green; and Rural: orange). Cyan dots represent the METAR stations used in Sect. S1 in the Supplement.

the Middle East. Its outputs are mass conservative interpolated to the CMAQ Lambert conformal conic grids at the required resolution and domain. After interpolating, the modeled PM_{10} concentration is calculated as the sum of Aitken, accumulation and coarse-mode modes from CMAQ, and the corresponding BSC-DREAM8bv2 bins with a diameter of less than or equal to 10 µm (Pay et al., 2012a).

2.3 Computational strategy

Running CALIOPE-AQFS at 4 and 1 km is a technical challenge. The simulations are run on the MareNostrum supercomputer (Intel Xeon E5-2670, 16 CPUs and 64 GB RAM memory per node) at BSC-CNS. Table 1 depicts the computational requirements for forecasting air quality at 48 h for each domain. The number of CPUs was chosen to maximize CPU efficiency. Thanks to the parallelization of meteorological and air quality models, MareNostrum uses up to 256 CPUs. Due to the variable nature and complex dependencies, the computational time for forecasting 48 h of

air quality fields for the 4 domains is 8–9 h. The most computationally demanding domain is AND, at 1 km resolution (666×358 cells, 256 CPU max., and 300 min). For the April 2013 simulation, times add up to 2880 CPU hours day^{-1}, or 86 400 CPU hours on a single processor (9.86 years). The storage for the April 2013 output files was 6.13 TB (~ 200 GB day^{-1}).

2.4 Evaluating the increase in resolution

A comparison of CALIOPE-AQFS model outputs and measurements was made for gas-phase and aerosol concentrations (O_3, NO_2, and PM_{10}). Representativeness continues to be a challenge when comparing gridded simulations to observational data at a point in time and space, as modeled concentrations represent a volumetric average over an entire grid cell. Furthermore, the stochastic compound embedded in the observations is not accounted for. Concerning temporal representativeness in the present comparison, both modeled and measured concentrations are averaged

Table 1. CALIOPE-AQFS computational requirements, in terms of central processor units (CPUs) and computational time (in min), for simulating 48 h air quality forecasts as a function of the domains IP-4 km (D2), AND-1 km (D3), BCN-1 km (D5) and MAD-1 km (D4), all of which are described in Fig. 1. D domains are described in Fig. 1.

	IP-4 km (399 × 399 cells)	AND-1 km (666 × 358 cells)	BCN-1 km (146 × 146 cells)	MAD-1 km (146 × 158 cells)
Meteorological modeling	128 CPU / 15 min	256 CPU / 80 min	128 CPU / 20 min	128 CPU / 20 min
Emissions modeling	1 CPU / 4 min	1 CPU / 4 min	1 CPU / 1 min	1 CPU / 1 min
Air quality modeling	256 CPU / 210 min	256 CPU / 220 min	128 CPU / 150 min	128 CPU / 110 min

hourly. CALIOPE-AQFS operationally receives air quality measurements from Spanish administrative networks in near-real time (NRT) without any quality control. For the present study, NRT measurements are filtered by removing data before and after measurement interruptions or calibrations. Also, a minimum cut-off threshold of $1\,\mu g\,m^{-3}$ is applied to the observed concentrations in order to avoid unrealistic observations. After filtering, the number of stations is 48/30/36 for O_3, 51/42/42 for NO_2, and 52/15/33 for PM_{10} in the AND/BCN/MAD domains, respectively.

The meteorological fields are evaluated for wind speed (U10) and wind direction (WD10) at 10 m, and for temperature at 2 m (T2M). The 10 METAR stations are all located at airports (6/2/2 stations in AND/BCN/MAD), and are discussed in Sect. S1 in the Supplement.

Figure 2 shows the location of the air quality and METAR (METeorological Aerodrome Report) stations over the respective domains. The spatial representativeness of the air quality network is highly variable. The influence of the station type is based on two classifications of air quality monitoring stations, the environment type (rural, R; suburban, S; and urban, U), and the dominant emissions source (traffic, T; industrial, I; and background, B). These were derived from council decision 97/100/EC (Garber et al., 2002).

The evaluation is based on discrete statistics performed on an hourly basis. We consider the correlation coefficient (r, Eq. A1), mean (absolute, relative, and fractional) biases (MB, MNBE, and MFB; Eqs. A2–A4), and error (MAE, MNGE, and MFE; Eqs. A5–A7). The root mean square error (rmse, Eq. A8) is also calculated, because it intensifies large differences between measured and observed concentrations (Table A1).

In order to evaluate the effect of increased resolution on forecast exceedances and non-exceedances of limit values established by the European legislation, we calculate categorical statistics based on comparisons with fixed concentration thresholds (T). The calculated statistics are accuracy (A, Eq. A9), bias (B, Eq. A10), probability of detection (POD, Eq. A12), critical success index (CSI, Eq. A11), and false alarm ratio (FAR, Eq. A13), whose formulas and descriptions are provided in Table A2 and also in Kang et al. (2005) and Eder et al. (2006). The 2008/50/EC Directive sets an information threshold of $180\,\mu g\,m^{-3}$ for maximum daily O_3

concentrations (Max 1 h O_3) and a target value of $120\,\mu g\,m^{-3}$ for the maximum daily 8 h running O_3 mean (Max 8 h O_3), which should not be exceeded more than 25 days per year. It establishes a limit value of $200\,\mu g\,m^{-3}$ for maximum daily NO_2 concentrations (Max 1 h NO_2), and $50\,\mu g\,m^{-3}$ for the daily PM_{10} mean (Mean 24 h PM_{10}), which should not be exceeded more than 35 times per year. Therefore, categorical evaluations will be performed for Max 1 h NO_2, Max 1 h and Max 8 h O_3, and Mean 24 h PM_{10}. Note that mean and maximum concentrations are calculated by considering at least 75 % of the data in the corresponding time base, i.e., values of at least 18 h per day for Mean 24 h, Max 1 h, and Max 8 h, and 6 h for 8 h values, as established by 2008/50/EC.

3 Concentration maps and spatial representativeness

To analyze the spatial differences between resolutions, Figs. 3, 4, and 5 show the monthly mean concentration maps for April 2013 over the MAD, BCN and AND domains at 4 km (left panels) and 1 km (right panels) for NO_2, O_3, and PM_{10}, respectively.

The maps of NO_2 and PM_{10} at both resolutions display similar distributions along the MAD and BCN urban plumes. On-road traffic constitutes the main source of primary pollutants in MAD and BCN. HERMESv2.0 estimates that 75 and 59 % of NO_x emissions are produced by on-road traffic in both domains, respectively. Consequently, when the resolution increases, the monthly mean O_3 concentration maps are almost identical, although the NO_x titration effect on O_3 is significant along highways and major point sources. In AND, NO_2 and O_3 concentrations are also conserved between resolutions along the shipping route crossing the Strait of Gibraltar towards the Mediterranean Sea.

However, the definitions of NO_2 concentrations along highways connecting the biggest cities to the rest of the country and industrial sectors are more easily identified at 1 km simulations than at 4 km, especially along those roads from/to Barcelona (e.g., the AP7 Mediterranean highway and the C32, which connect the harbor and the airport) and Madrid (the A-2 and A-6 in the north, and the A-3, A-4 and A-5 in the south). In the same way, 1 km O_3 maps are more textured than those at 4 km along highways, because the titration effect is more significant at 1 km, due to less dilution
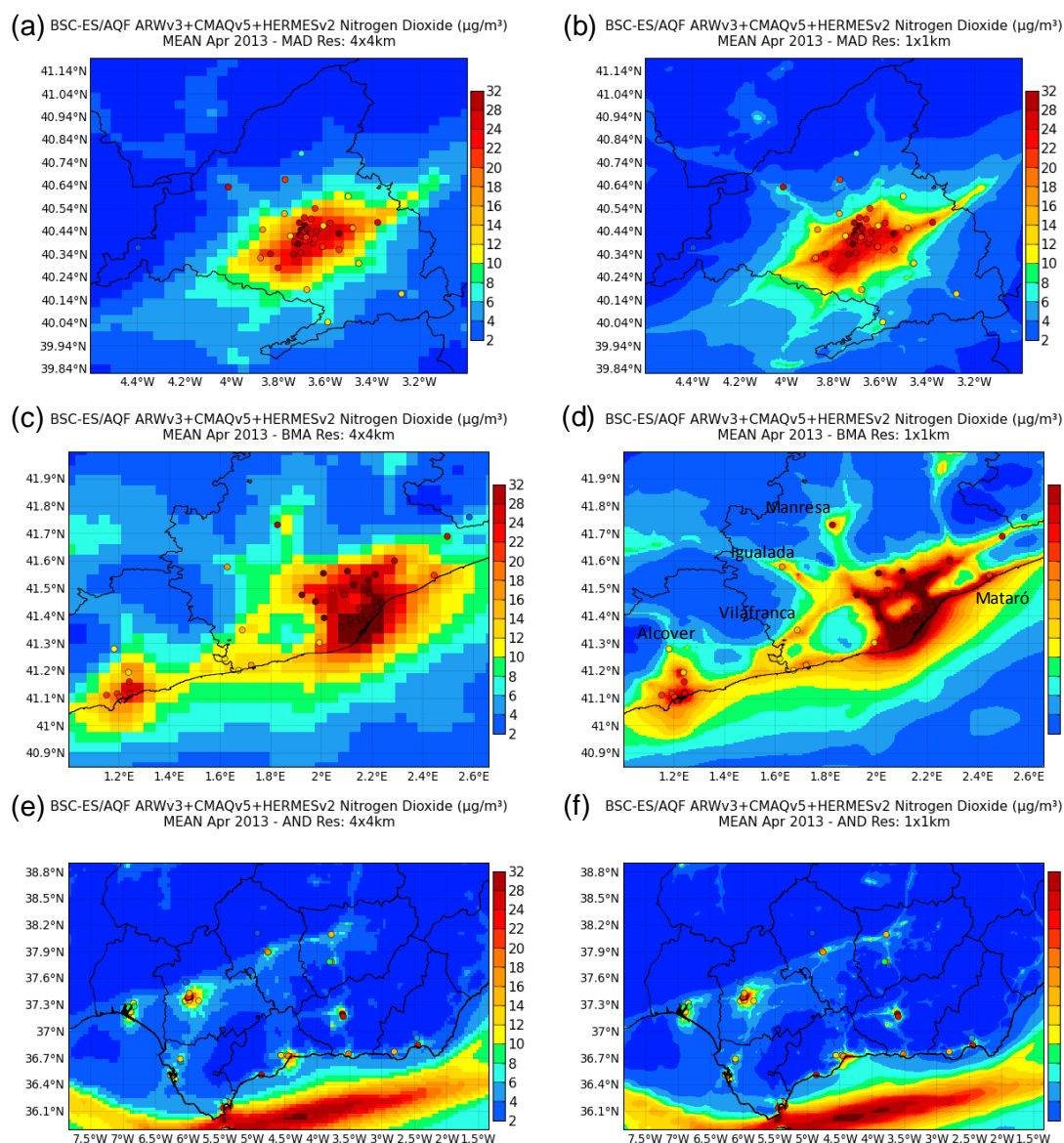
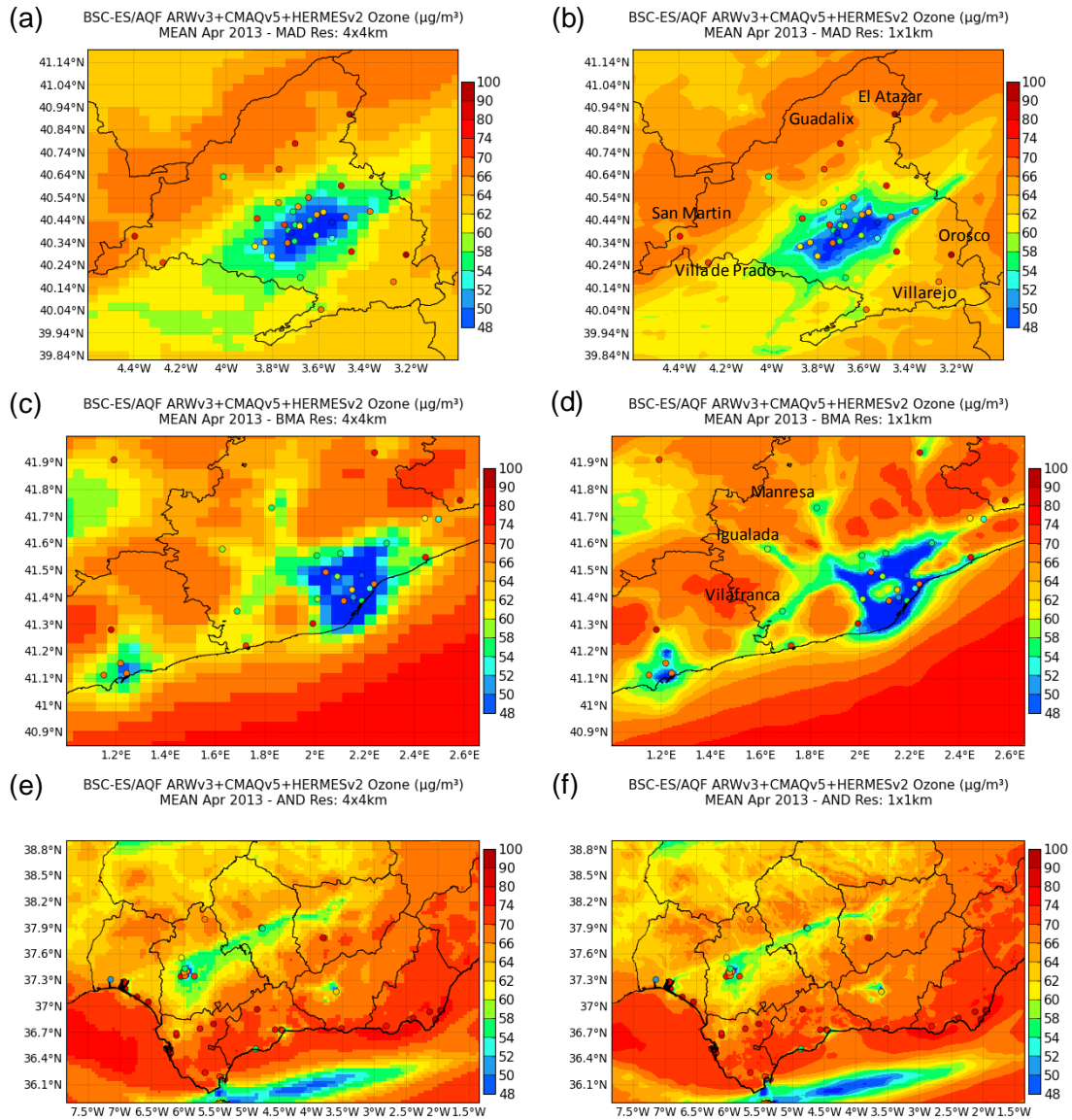**Figure 3.** CALIOPE-AQFS mean NO_2 concentrations ($\mu g\,m^{-3}$) in April 2013 over **(a, b)** MAD, **(c, d)** BCN, and **(e, f)** AND, as a function of horizontal resolution: 4 km (left column) and 1 km (right column). Dots indicate the mean concentrations at the air quality stations.

within grid cells. The titration effect of NO_x on O_3 over the main sources is more forceful in BCN than in MAD, given that BCN has a larger concentration gradient resulting from complex topography and recirculation flows that accumulate pollutants.

The improvement in the definition along roads in AND is lower than that observed in the MAD and BCN domains, due to the fact that the AND domain is bigger and displays lower traffic emission sources than the MAD or BCN domains. Regarding PM_{10}, the main component in AND is the desert dust ($\sim 40\,\%$ in both resolutions) from North Africa. This is because there were two episodes on 14–19 and 25–26 April that affected the IP, as shown by the S–N PM_{10} gradient (Fig. 5e

and f). The desert dust is transported from long-range simulations with BSC-DREAM8bv2.

Over complex terrains, the 1 km simulation produces more realistic looking NO_2 concentration maps because of its more detailed topographic information. For instance, the BCN 1 km simulation displays the lowest NO_2 concentrations ($< 10\,\mu g\,m^{-3}$) along the coastal chain (500 m in height) and pre-coastal chain (1000–1700 m in height), except for the city's urban hill, where concentrations reach 20–40 $\mu g\,m^{-3}$. In contrast, the 4-km simulation provides smoother NO_2 concentrations without any concentration gradient. Thus, the 1-km simulation generates slightly higher O_3 background concentrations than the 4-km simulation along

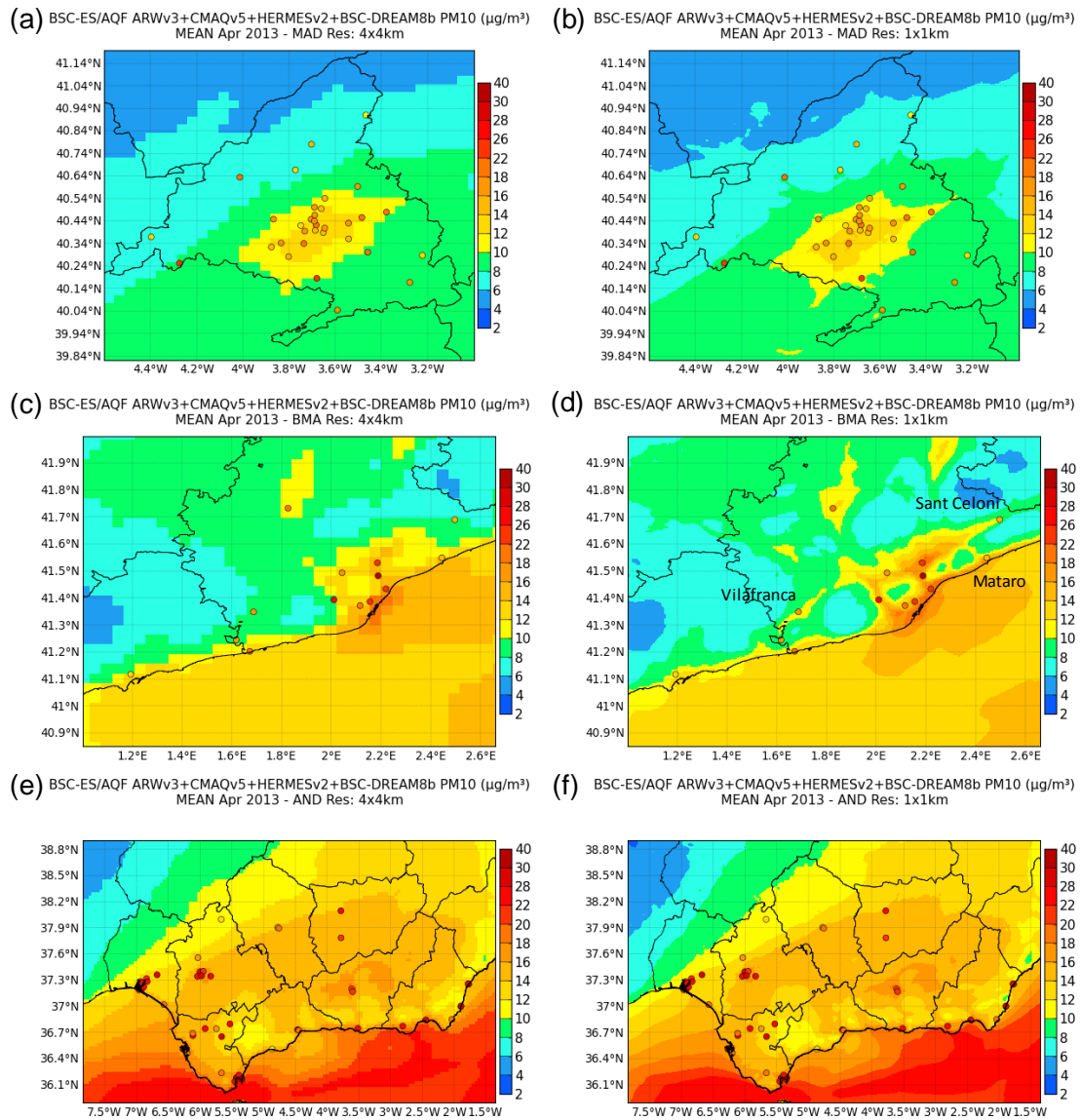**Figure 4.** CALIOPE-AQFS mean O_3 concentrations ($\mu g\,m^{-3}$) in April 2013 over **(a, b)** MAD, **(c, d)** BCN, and **(e, f)** AND, as a function of horizontal resolution: 4 km (left column) and 1 km (right column). Dots indicate the mean concentrations at the air quality stations.

the BCN pre-coastal chain (66–70 vs. 70–74 $\mu g\,m^{-3}$), as well as across the Iberian Massif (AND), where the O_3 displays a significant structure due to the higher-resolution topography that follows the basin and the areas of high-density on-road traffic.

Figures 3, 4, and 5 include dots corresponding to mean concentrations at air quality stations that help qualitatively to evaluate the modeled spatial representativeness at both resolutions. Note the strong correlation between NO_2 observations and the 1-km simulation near the primary suburban traffic roads in BCN (e.g., Vilafranca, Igualada, Manresa, and Mataró). Regarding O_3, although observed concentrations depict an overall tendency of the model to underestimate concentrations at both resolutions, the 1-km simulation shows

better agreement with measurements at rural background stations (e.g., the El Atazar, San Martín, Villa de Prado, Villarejo and Orosco stations in MAD), and at suburban traffic stations (e.g., Manresa, Igualada and Vilafranca in BCN, with modeled O_3 concentrations of around 54–58 $\mu g\,m^{-3}$ at 1 km, and 60–66 $\mu g\,m^{-3}$ at 4 km). For PM_{10}, comparisons with measurements show that modeled concentrations are underestimated over background areas, mainly outside the urban/suburban areas, as already discussed in Pay et al. (2012a). However, PM_{10} measurements at the urban/suburban stations of Vilafranca, Sant Celoni, and Mataró in BCN (14–16 $\mu g\,m^{-3}$) show a higher correlation at 1 km than at 4 km (12–14 $\mu g\,m^{-3}$ vs. 8–10 $\mu g\,m^{-3}$).
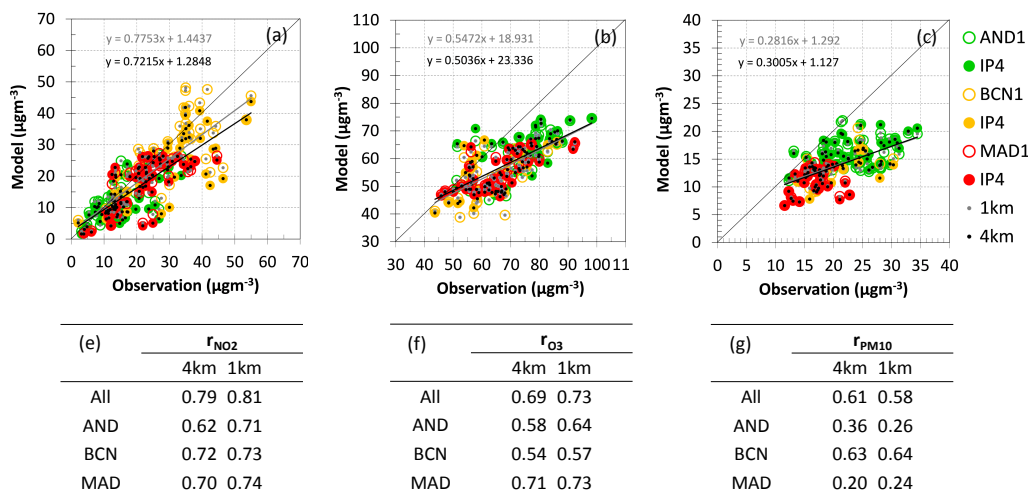
Figure 5. CALIOPE-AQFS mean PM_{10} concentrations ($\mu g\,m^{-3}$) in April 2013 over **(a, b)** MAD, **(c, d)** BCN, and **(e, f)** AND, as a function of horizontal resolution: 4 km (left column) and 1 km (right column). Dots indicate the mean concentrations at the air quality stations.

The spatial variability of the increased resolution is analyzed quantitatively by means of concentration maps, shown in Fig. 6 for NO_2, O_3 and PM_{10} over AND, BCN and MAD. Over all the domains, the correlation improves as a function of the resolution increase for NO_2 and O_3, indicated by the increase in monthly r from 0.79 (4 km) to 0.81 (1 km) for NO_2, and from 0.69 to 0.73 for O_3. The slopes improve with the resolution increase, from 0.72 (4 km) to 0.77 (1 km) for NO_2, and from 0.50 (4 km) to 0.54 (1 km) for O_3. This results from the improved model performance at urban stations, indicating that CALIOPE-AQFS captures the magnitude of the variability between urban regions better at 1 km than at 4 km. In contrast, for PM_{10}, the monthly r decreases from 0.67 to 0.58 when the resolution increases. While the PM_{10} spatial

variability over BCN and MAD improves when the resolution increases (r increases by 0.01 and 0.04, respectively), the global correlation coefficient decreases at the AND stations (52/100) by 0.1, from 0.36 (4 km) to 0.26 (1 km). Despite the unfavorable effect of the resolution increase in PM_{10} over AND, the NO_2 and O_3 concentrations show the highest absolute increases for the spatial r over this domain, from 0.62 (4 km) to 0.71 (1 km) for NO_2, and from 0.58 (4 km) to 0.64 (1 km) for O_3 (increasing r by 0.09 and 0.06, respectively).

Figure 6. Monthly mean scatter plots for CALIOPE-AQFS (y axis) and observed (x axis) concentrations for the three study domains (AND in green, BCN in yellow, and MAD in red), as functions of horizontal resolution for **(a)** NO_2, **(b)** O_3 and **(c)** PM_{10}. Equations show the linear adjustment between models and observations at 1 km (light grey) and 4 km (dark grey). Spatial correlation coefficients as a function of resolution and domain are shown for **(e)** NO_2, **(f)** O_3, and **(g)** PM_{10}.

4 Temporal evaluation

4.1 Pollutant

Table 2 presents the statistical evaluation by pollutant, with a focus on the reproduction of high concentrations established by the European directive (2008/50/EC). Depending on the pollutant's lifetime and variability, as well as its dependency on precursors, increased resolution shows different impacts. The resolution increase has a positive effect on NO_2, decreasing its bias by 2.0 $\mu g\,m^{-3}$ (from -4.5 to $-2.5\,\mu g\,m^{-3}$), but it also increases the absolute (squared) error by 0.3 to 0.9 $\mu g\,m^{-3}$. This positive effect is sustained by the relative variability, where the MB (MFB) is reduced by 42 % (19 %), and MAE (MFE) only increases by 2 % (1 %). The r does not change between resolutions ($r = 0.54$), partially due to the fact that the NO_2 is a primary pollutant, and emissions at both resolutions are modeled using the same approach. The bias improvement at 1 km resolution is justified, because in theory the higher resolution leads to better emissions allocation from point, linear or area sources, decreases the artificial dilution of emissions compared to the larger grid area, and, due to the decrease in artificial dilution, treats chemistry more properly near large emission sources.

In contrast, the resolution increase has a negative effect on hourly and Max 8 h O_3 concentrations, increasing the bias and error by 0.1–0.8 $\mu g\,m^{-3}$. Relative (fractional) bias and error increase by 8 % (15 %) and 1 % (1 %), respectively, for hourly O_3, and by 6 and 4 % for Max 1 h O_3.

According to the categorical evaluation, only a few exceedances of the European target and limit values were detected for Max 1 h NO_2 (9), Max 1 h O_3 (25), and Mean 24 PM_{10} (31) in April 2013. Thus, a categorical evaluation

is performed on the temporal basis established by the European legislation, but it uses a T based on the 75th percentile (75p) of the observed concentrations in each case, where T is 71 $\mu g\,m^{-3}$ for Max 1 h NO_2, 108 (101) $\mu g\,m^{-3}$ for Max 1 h (Max 8 h) O_3, and 27 $\mu g\,m^{-3}$ for Mean 24 h PM_{10}.

Overall, CALIOPE-AQFS underestimates exceedances at both resolutions, indicating that errors of missing observed exceedances are not completely resolved by increasing the horizontal resolution ($a < d$). The best performance is found for Max 1 h NO_2, where categorical bias (B, Eq. A10) improves from 37 % (4 km) to 40 % (1 km), although the tendency to underestimate exceedances remains with the resolution increase ($B < 100$ %).

For NO_2 Max 1 h, there are 953 observed exceedances ($b + d$) of the threshold ($T = 47\,\mu g\,m^{-3}$). Increasing the resolution increases the POD from 49 % (4 km) to 56 % (1 km). As with POD, CSI examines the exceedances, but in a more comprehensive way, by considering both false alarms and missing events. POD and CSI increase by 14 and 20 %, respectively, when the resolution is increased from 4 to 1 km. For O_3, POD has a relatively low POD value, and it decreases as the resolution increases. Of the 1306 observed exceedances of the 108 $\mu g\,m^{-3}$ Max 1 h, CALIOPE-AQFS detected 112 exceedances at 4 km and only 96 at 1 km. Increasing resolution decreases POD and CSI by 22 and 25 % for O_3 Max 1 h, whereas they do not significantly change for Max 8 h O_3 and Mean 24 h PM_{10}.

FAR increases for Max 1 h NO_2 (from 40 % to 42 %) and decreases for Max 1 h O_3 (from 27 to 17 %), when the resolution increases. In relative terms, this variability is more significant for Max 1h O_3 (37 %) than for Max 1 h NO_2 (5 %), indicating that, in terms of failures, the resolution has a positive global effect by reducing false exceedances.

Table 2. Discrete and categorical statistics for NO_2, O_3, O_3-8 h, and PM_{10} for April 2013 as functions of horizontal resolution (4 and 1 km). n indicates the number of pairs of data used in the discrete evaluation on an hourly basis. OM and MM depict the measured and modeled mean concentrations, respectively. T is the threshold applied in the categorical evaluation. Max 1 h and mean 24 h concentrations are calculated by considering more than 75 % of the hours in a day, as established by Directive 2008/50/EC.

	NO_2		O_3		O_3-8 h		PM_{10}	
n (stations)	90 761 (135)		76 471 (114)		3248 (114)		66 642 (100)	
OM ($\mu g\,m^{-3}$)	22.0		68.4		88.6		20.6	
EU LV/TV ($\mu g\,m^{-3}$) (temp. basis)	200 (Max 1 h)		180 (Max 1 h)		120 (Max 8 h)		50 (Mean 24 h)	
EU LV/TV exceedances	0		25		0		31	
T^* ($\mu g\,m^{-3}$) (temp. basis)	71 (Max 1 h)		108 (Max 1 h)		101 (Max 8 h)		27 (Mean 24 h)	
	Discrete evaluation							
	4 km	1 km	4 km	1 km	4 km	1 km	4 km	1 km
MM ($\mu g\,m^{-3}$)	17.4	19.3	58.0	57.3	72.4	71.5	13.9	14.0
r	0.54	0.54	0.61	0.61	0.54	0.51	0.45	0.44
MB ($\mu g\,m^{-3}$)	−4.5	−2.6	−10.5	−11.3	−16.3	−17.2	−6.7	−6.6
MAE ($\mu g\,m^{-3}$)	12.9	13.2	19.7	19.8	18.4	19.2	12.6	12.7
rmse ($\mu g\,m^{-3}$)	19.8	20.4	24.6	24.7	21.8	22.8	17.2	17.4
MNBE (%)	−20.4	−11.8	−15.3	−16.5	−18.4	−19.4	−32.5	−32.0
MNGE (%)	58.5	59.9	28.8	28.9	20.8	21.7	61.1	61.6
MFB (%)	−28.5	−23	−13.1	−15.1	−19.3	−20.5	−63.3	−64.1
MFE (%)	69.2	68.7	37.1	37.4	22.5	23.5	85.7	87.1
	Categorical evaluation (threshold = T^*)							
	4 km	1 km	4 km	1 km	4 km	1 km	4 km	1 km
a (false alarm)	306	384	41	19	17	6	131	133
b (hits)	466	537	112	96	6	4	331	334
c (correct negative)	2517	2439	1846	1868	2826	2837	1978	1976
d (misses)	487	416	1194	1210	399	401	334	331
B (%, 100)	37	40	8	7	1	1	42	42
POD (%, 100)	49	56	9	7	1	1	50	50
CSI (%, 100)	81	97	12	9	6	2	69	70
FAR (%, 0)	40	42	27	17	74	60	28	28
A (%, 100)	79	79	61	62	87	87	83	83

T^* is defined as 75p of the observed concentrations estimated temporally, as established by EU Directive 2008/50/EC.

For various reasons, accuracy (A) remains almost constant when the resolution increases. For NO_2 and O_3, this is due to a stable sum of b and c, increasing b at the cost of c, and vice versa. For NO_2, the number of hits (b) to forecast Max 1 h at 1 km is higher than 4 km (537 vs. 466), but the number of correct negatives at 1 km is lower than at 4 km (2439 vs. 2517). The resolution increase has the opposite effect on O_3, decreasing the number of hits by 14 % for Max 1 h and 33 % for Max 8 h. The increase in the number of correct negatives is less than 2 % in both Max 1 h and Max 8 h O_3.

4.2 PM_{10} components

The resolution increase has the lowest effect on PM_{10} hourly concentrations and its exceedances (< 1 %). PM_{10} components are secondary inorganic aerosols (SIA), which include sulfate ($SO_4 = SO_4^{2-}$), nitrate ($NO_3 = NO_3^-$), ammonium

($NH_4 = NH_4^+$), SOA, elemental carbon (EC), sea salt (SS), desert dust (DD), and primary PM (PPM).

Pay et al. (2012a) evaluated the PM components at some urban and rural background stations in Spain using the CALIOPE-AQFS based on CMAQv4.5, where they showed that the model underestimated SIA by a factor of 2–3. The highest underestimation was found for fine carbonaceous aerosols (a factor of 4), in part related to the state of the science concerning SOA formation pathways. The updated version of CMAQ, v5.0.1 includes scientific improvements to SOA formation and aerosol dynamics, which could improve the modeled PM_{10} performance and its components.

Figure 8a shows that the resolution increase does not significantly change the PM_{10} composition. DD remains the main contributor ($\sim$ 40–41 %), followed by PPM (22–24 %), SIA ($\sim$ 21–22 %), SS (9–11 %), EC ($\sim$ 4 %) and SOA ($\sim$ 0.6 %). However, the effect of the increased resolution on
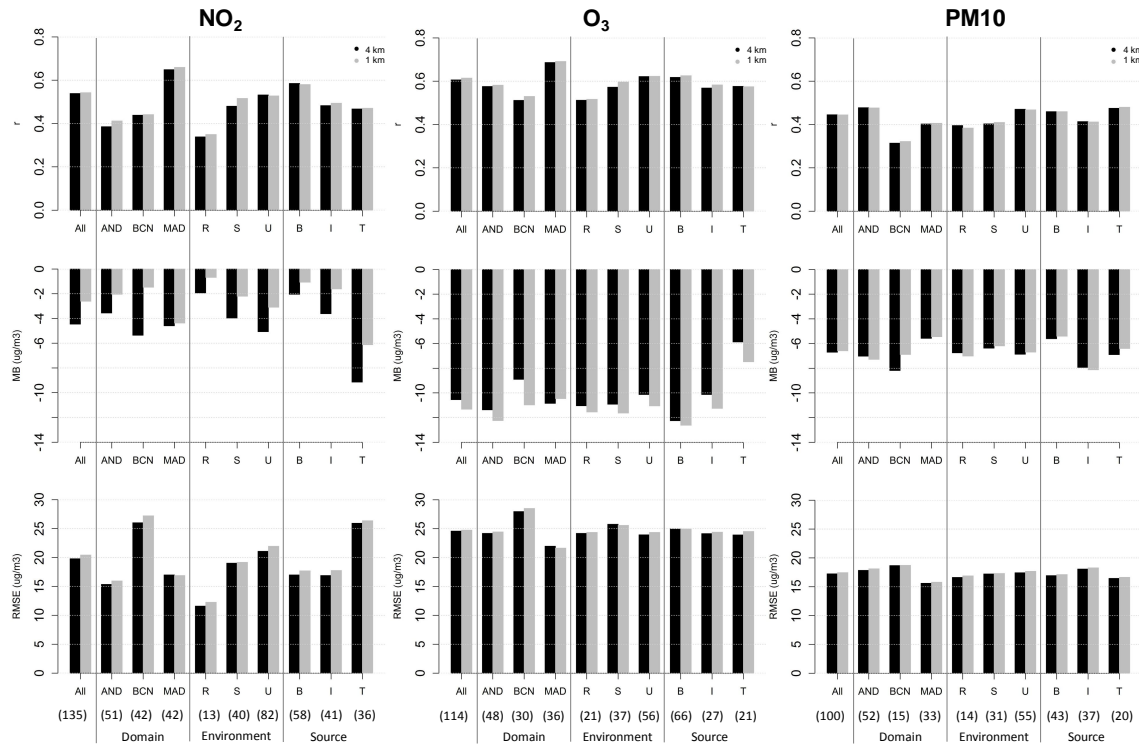
Figure 7. Statistics (r, MB, and rmse in the rows) for each pollutant (NO_2, O_3, and PM_{10} in the columns) on an hourly basis as a function of horizontal resolution: 4 km (black) and 1 km (grey). Four categories are considered: all stations (all), domain (AND, BCN and MAD), station environment (R, S, and U), and main sources (B, I, and T).

PM_{10} component concentrations is different (Fig. 8b), depending on their origin, atmospheric cycle and the way they are modeled. DD concentrations do not change between resolutions, because they are mass conservative when interpolated from $0.5° \times 0.5°$ to $1\,km \times 1\,km$.

For SIA, increasing the resolution increases NO_3 and NH_4 concentrations by 4 and $\sim 2\,\%$, respectively, and it decreases SO_4 by $\sim 2\,\%$. The NH_4 increase means there are more primary precursors (H_2SO_4 or HNO_3 / NO_2) available to neutralize NH_3 (gas) to NH_4 (aerosol). However, the variability between SO_4 and NO_3 is more difficult to explain, due to the nonlinearity of photochemistry and aerosol formation, which is controlled to some extent by the ISORROPIA thermodynamic equilibrium. Furthermore, the absence of aerosol measurements for April 2013 does not allow us to investigate this further.

The resolution increase results in a decrease in SS of $\sim 16\,\%$, the largest change of all the PM_{10} components. CMAQv5.0.1 simulates SS emission as a function of the wind speed and the relative humidity (Gong, 2003; Zhang et al., 2005). Although not shown here, when the resolution increases, the wind speed decreases at the available PM_{10} stations by $\sim 1.4/0.4/0.2\,m\,s^{-1}$ over AND/BCN/MAD, and also over the open ocean.

For primary PM components EC and PPM, increasing resolution results in higher concentrations (by 10 and $\sim 12\,\%$,

respectively). As for NO_2, the 1 km simulation leads to a reduced effect of artificial dilution of emissions in a grid cell, so concentration gradients are stronger than in the 4-km simulation.

4.3 Domain

The resolution increase has varying impacts due to differences in geographical location and emissions patterns over the domains (Fig. 7). BCN shows the highest NO_2 bias decrease (73 %) when the resolution increases, but no effect on the correlation (< 7 %). However, O_3 shows significant variability over BCN, increasing r by 4 % and MB by 23 %. To a lesser extent, MB also increases over AND (by 8 %). Meanwhile, the variability over MAD is reduced (bias differences less than 4 %). MB decreases for PM_{10} (bias differences less than $1\,\mu g\,m^{-3}$) over the urban domains of MAD (3 %) and BCN (16 %), and increases over AND (7 %).

Figure 9 analyzes the impact of the resolution increase on daily cycles. Although PBL measurements are not available, PBL daily cycles are displayed together in order to find some correlations with the daily pollutant variability. Due to the lamination of PBL growth by the Mediterranean Sea breezes, the PBL reaches its maximum height at midday, being the highest in MAD (1600 m a.g.l.), followed by AND (1000 m a.g.l.) and BCN (900 m a.g.l.).
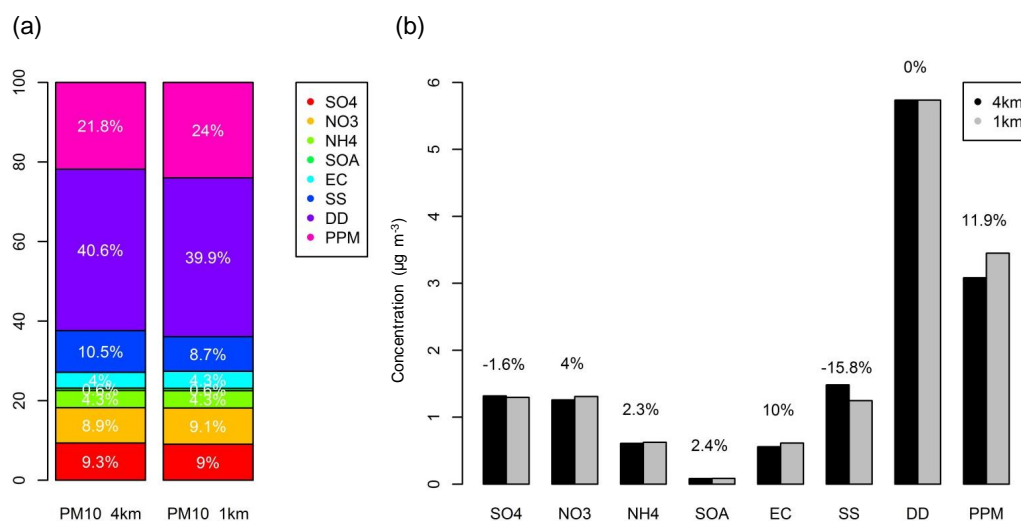
Figure 8. Resolution effect on PM_{10} components in April 2013. **(a)** Percentage of PM_{10} components: sulfate (SO_4), nitrate (NO_3), ammonium (NH_4), secondary organic aerosol (SOA), elemental carbon (EC), sea salt (SS), desert dust (DD), and primary particulate matter (PPM). **(b)** PM_{10} component concentrations in the 1 km simulation (black) and 4 km simulation (grey). Numbers over bars indicate the % increase when increasing the resolution.

As shown in Sect. S1 in the Supplement, the pollutant transport in the BCN coastal domain is controlled by mesoscale phenomena such as sea breezes (day) and land breezes (night), which are a result of its complex topography and location (Baldasano et al., 1994; Millán et al., 1997; Gonçalves et al., 2009). The NO_2 daily cycle is highly influenced by traffic emissions (Fig. 9). Both resolutions show the highest underestimations for the morning peak (6 a.m.) ($\sim 20\,\mu g\,m^{-3}$). Although the afternoon peak is well reproduced, there is excessive variability at both resolutions, a result of problems with the wind direction. During the sea breeze period, the mean simulated wind was more easterly than westerly, as registered by measurements (Sect. S1 in the Supplement). Several works indicate that WRF has difficulty reproducing the morning and evening transition over the urban environment, possibly because it does not model the heat retention in cities (Makar et al., 2006; Appel et al., 2013). Increasing the resolution increases NO_2 concentrations by 21 %, from $14\,\mu g\,m^{-3}$ (4 km) to $17\,\mu g\,m^{-3}$ (1 km) during the morning hours after sunrise (5–9 a.m.), and in the evening hours after sunset (5–9 p.m.). This behavior could be explained by PBL variability when increasing the resolution, which decreases PBL height by $\sim 33\,m$ for these hours.

NO_2 performance impacts the O_3 daily cycles over BCN, showing that 4 and 1 km simulations underestimate maximum O_3 concentrations by $\sim 20\,\mu g\,m^{-3}$ at midday (1–4 p.m.) and overestimate minimum O_3 concentrations by $\sim 20\,\mu g\,m^{-3}$ in the morning hours after sunrise (5–9 a.m.). The resolution increase results in slightly lower O_3 concentrations at night, which is perhaps the result of lower PBL heights in the 1-km simulation during the early morning and late afternoon, when the PBL height tends to be the

lowest. During these hours, the titration effect of NO_2 on O_3 is greater, improving the O_3 overestimation of the daily minimum, which allows a slightly higher hourly r (2 %). However, O_3 underestimation increases in the late afternoon, contributing to an increase in the hourly mean bias from $\sim 9\,\mu g\,m^{-3}$ (4 km) to $\sim 11\,\mu g\,m^{-3}$ (1 km).

In BCN, the PM_{10} underestimation is not systematic throughout the daily cycle (Fig. 9), which shows a bias of ~ 20 (10) $\mu g\,m^{-3}$ at day (night) time. The higher daytime underestimation as compared to the nighttime cannot be explained by the current results, but it could be a result of missing sources (e.g., fugitive agricultural emissions and wind-blown dust), problems with PBL height overestimation, and an excess dilution of emissions. The resolution increase reduces the bias by $\sim 1\,\mu g\,m^{-3}$ (16 %), especially during early morning and late afternoon, when the highest PBL height variability between resolutions is observed. Although the evaluation of T2M, U10 and WD10 indicates that the resolution increase has a small effect over BCN (Sect. S1 in the Supplement), the reduction of the artificial dilution of NO_2 emissions – together with a lower PBL height at 1 km than at 4 km during the night and early morning – improves NO_2, O_3 and PM_{10} concentrations, which in turn decreases their biases.

For AND, the model underestimates observed NO_2 concentrations throughout the daily cycle by $\sim 5\,\mu g\,m^{-3}$ for both the 4 and 1 km simulations, with the highest underestimation during the morning peak ($\sim 25\,\mu g\,m^{-3}$) and the lowest during the afternoon peak ($\sim 10\,\mu g\,m^{-3}$). The resolution increase reduces the bias from -3.5 to $-2\,\mu g\,m^{-3}$ (by 43 %) and increases r by 7 % (from 0.39 to 0.41). As in BCN, the NO_2 underestimation directly impacts the O_3 daily cycle
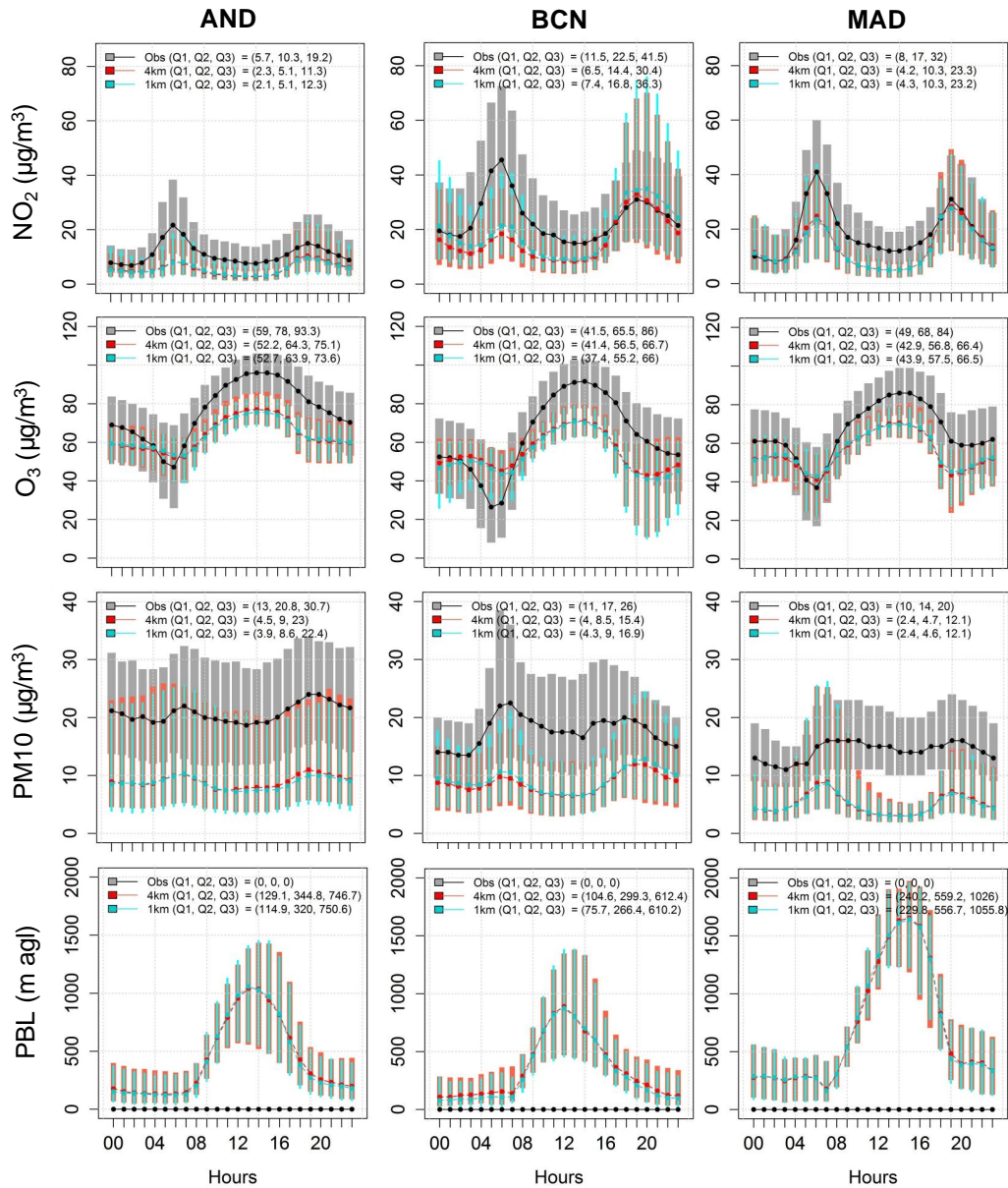
Figure 9. Daily cycles for NO_2, O_3 and PM_{10} for each study domain at available stations as a function of resolution. No observations of PBL are available. Q1, Q2 and Q3 indicate quartiles for the daily cycle. Bars show Q1 and Q3 at each hour.

(which the resolution increase cannot resolve), increasing the bias by $\sim 1\,\mu g\,m^{-3}$, a phenomenon that is predominant in the morning hours. In the case of PM_{10}, the daily cycle indicates that the biases are almost systematic throughout the day ($\sim 22\,\mu g\,m^{-3}$). Increasing the resolution increases the bias by less than 4 % in the late afternoon, which is perhaps dominated by the decrease in PBL height. When the resolution is increased, NO_2 performs better, partially due to the improved model performance for the temperature and wind speed (Sect. S1), as well as the lower nighttime and higher daytime PBL. Meanwhile, the O_3 and PM_{10} performances do not change significantly.

During April 2013, the main flow over MAD was controlled by S–SW synoptic winds channeled by orographic barriers in the NW domain and the Tajo Valley (Valverde et al., 2014). The NO_2 daily cycle depicts a high influence of traffic emissions (Fig. 9), showing significant model underestimation at both resolutions for the morning/afternoon peaks ($\sim 15/10\,\mu g\,m^{-3}$). Note that, in terms of the temporal variability of the NO_2 concentrations, the model performs well at the afternoon peak, when the air flow is controlled by southeastern winds. The NO_2 performance leads to more accurate O_3 daily cycles than in AND and BCN, especially in the early morning, when the titration effect of
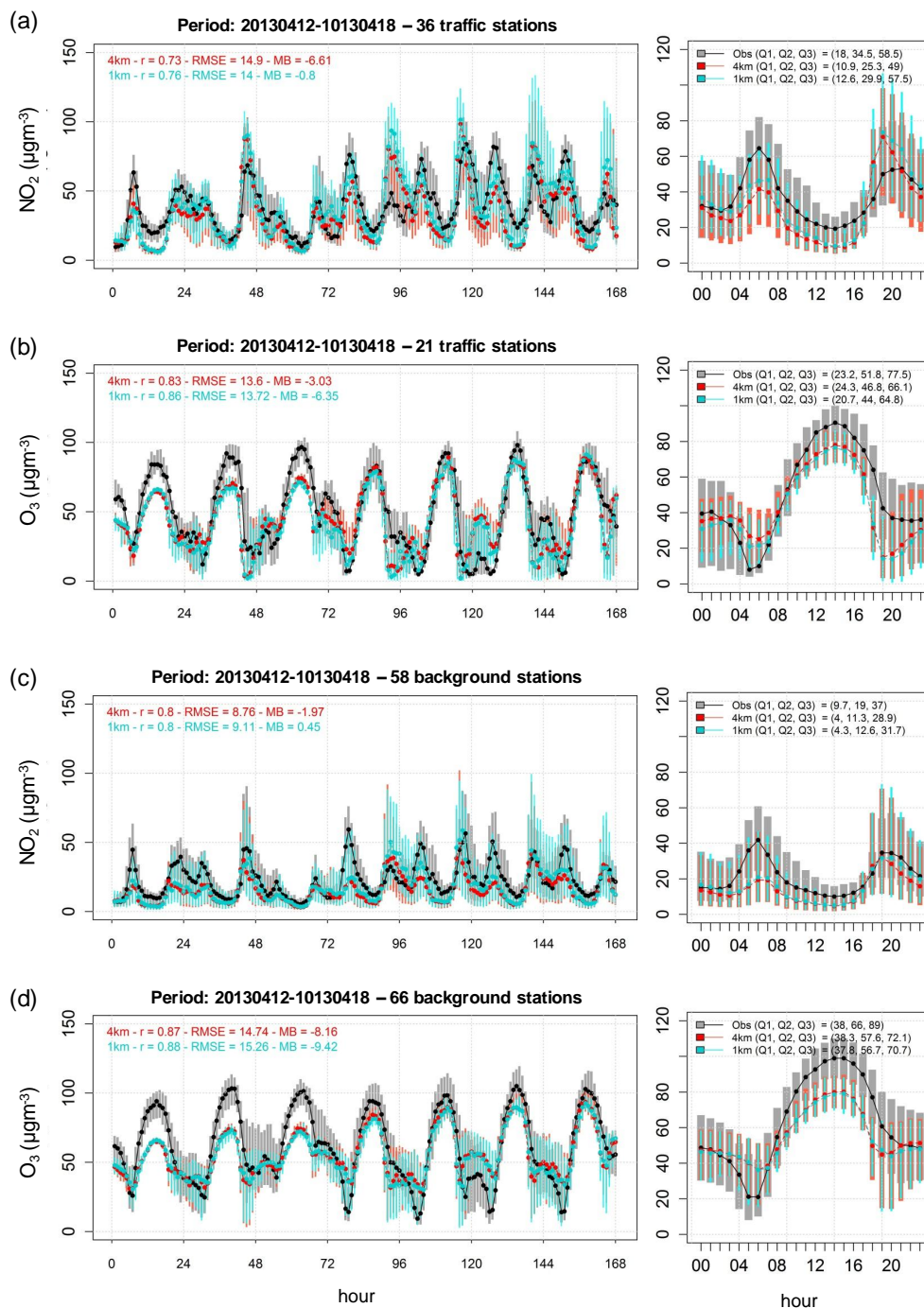
Figure 10. Temporal series and daily cycles for NO_2 and O_3 at background (a and b, respectively) and traffic stations (c and d, respectively) for the episode of 12–18 April 2013. Q1, Q2 and Q3 indicate quartiles for the daily cycle. Bars show Q1 and Q3 at each hour.

NO_2 is greater, because the NO_2 morning peak underestimation is smaller when compared to the other domains. Meanwhile, the modeled PM_{10} at both resolutions presents a profile controlled by traffic emissions. Observed concentrations display a flatter daily cycle, in which the model underestimation reaches $40\,\mu g\,m^{-3}$ in the morning. Increasing resolution shows a positive effect for NO_2 and PM_{10}, because

it increases r by 0.01 and reduces MB and the rmse by 0.1–$0.2\,\mu g\,m^{-3}$. However, it has the lowest variability when compared to the other domains (less than 5 % for bias, error and r), likely the result of a relatively simpler topography and meteorological patterns.

4.4 Environment and major sources

Figure 7 shows that the resolution impact also depends on the type of area and the dominant emission source. Theoretically, the meteorological fields of urban areas differ from those of surrounding rural areas, because of their different morphologies (radiation trapping and wind profiles), surface materials (heat storage) and variable energy consumption (heat release).

Increasing resolution reduces the NO_2 bias at suburban and urban stations by 1.8–2 $\mu g\,m^{-3}$, and to a lesser extent by 1.2 $\mu g\,m^{-3}$ at rural stations. The correlation coefficients also improve at suburban stations (from 0.48 to 0.52) and rural stations (from 0.34 to 0.35). This may be due to better allocation of land-use categories (urban vs. rural) and their fraction in a grid cell in the 1 km simulation than in the 4 km simulation. The NO_2 bias decreases by 39 % (65 %) at urban (background) stations, but O_3 biases increase by 9 % (5 %). For PM_{10}, the resolution increase does not significantly change as a function of area type, with differences in bias and error of less than ± 4 % ($< 0.5\,\mu g\,m^{-3}$) between the two resolutions.

The low improvement at urban stations may be because the NoahLSM land-surface model does not consider the effect of urban morphology or thermal parameters in order to model meteorological fields accurately. Modeling air quality on an urban scale over cities requires a description of the heat–momentum exchange between buildings and the lower atmospheric layers. For instance, the impact of using an urban model on meteorological fields over the greater Paris area was studied by Kim et al. (2013) using WRF with the urban canopy model, demonstrating that below 1 km in height, overestimations of wind speed were significantly reduced.

The impact on r of increasing resolution is less than 2 % for primary pollutants near important emissions sources. For example, it reduces NO_2 biases at traffic (industrial) stations by $\sim 3\,\mu g\,m^{-3}$ (2 $\mu g\,m^{-3}$), but it increases O_3 biases by $\sim 2\,\mu g\,m^{-3}$ (1 $\mu g\,m^{-3}$). However, the resolution increase in the range of 4–1 km does not exhibit the expected improvement in the hourly statistics that are based on the constraints of the current model formulation. In other words, it cannot resolve the subgrid air quality variability merely by increasing resolution. For instance, although on-road traffic emissions are estimated by following a bottom-up approach along highways and routes, heterogeneity is lost in the CTM volume-averaging process, which artificially dilutes emissions rates over the grid cells. The resolution effect is low at background stations, which generally are not influenced by any single source, but rather by the integrated contribution from all sources upwind of the stations where variations are less than 1 % for O_3 and PM_{10} ($< 1\,\mu g\,m^{-3}$). However, background NO_2 levels increase by $\sim 1\,\mu g\,m^{-3}$ (48 %) from 4 km to 1 km.

Figure 10 shows the temporal series and daily cycles for NO_2 and O_3 at traffic and background stations throughout the episode of 12–18 April 2013. At traffic stations, the temporal series show a remarkable O_3 daily cycle (observed 25p $= 23.2\,\mu g\,m^{-3}$ and 75p $= 77.5\,\mu g\,m^{-3}$), due to O_3 destruction caused by high NO_x levels (observed 50p $= 34.5\,\mu g\,m^{-3}$). In contrast, the NO_2-limited regime at background sites (observed 50p $= 19\,\mu g\,m^{-3}$) allows for higher O_3 concentrations (observed 25p $= 38\,\mu g\,m^{-3}$ and 75p $= 89\,\mu g\,m^{-3}$) than in high NO_2 environments.

During the episode mentioned above, the resolution increase at traffic stations had a positive effect by increasing the r for NO_2 (from 0.73 to 0.76) and O_3 (from 0.83 to 0.86), and also by decreasing the NO_2 mean bias by $\sim 5\,\mu g\,m^{-3}$ (from 6 to 1 $\mu g\,m^{-3}$). The NO_2 daily cycle improves in the morning hours after sunrise, reducing bias by 5–10 $\mu g\,m^{-3}$ and contributing to a reduction in O_3 overestimations ($\sim 5\,\mu g\,m^{-3}$). In contrast, at background stations, where the NO_x / O_3 chemistry is less dominant, the resolution effect is not significant. Such behavior indicates that a finer resolution improves the model performance, because horizontal resolution affects the representation of chemical processes near large emissions sources, such as the formation of O_3 and nighttime O_3 titration (Mathur et al., 2005).

5 Conclusions

The present work shows the effects of increasing the horizontal resolution from 4 km to 1 km using the CALIOPE-AQFS on pollutant concentrations (NO_2, O_3, and PM_{10}) over three Spanish domains (AND, BCN and MAD) in April 2013.

The global features of concentration maps at both resolutions are quite similar, with zones of high/low concentrations identically located, which is expected, since both simulations are based on the same emissions data set. Further comparisons demonstrate that increasing the resolution provides better-defined and more realistic concentration structures over large emission sources (roads and industries) and complex terrains (more sharply defined orographic hills). The titration effect on O_3 by NO_x along highways and major point sources is more evident in 1-km simulations than at 4 km, since NO_x concentrations tend to be higher in the 1 km simulation due to less dilution. This improvement is quantified by an increase in the spatial correlation coefficients of 3 % (6 %) for NO_2 (O_3).

However, the resolution increase in the range of 4 to 1 km does not exhibit the expected improvement in hourly statistics for any pollutant. Hourly correlation coefficients do not change significantly, and absolute (relative) errors and biases vary by less than 2 $\mu g\,m^{-3}$ (9 %). The merit of the resolution increase may be underrated when classical statistics are applied at measurement stations (Mass et al., 2002; Gego et al., 2005). For instance, although the structure of important NO_2 urban plume features ($> 40\,\mu g\,m^{-3}$) often becomes

more realistic (stronger and more defined plumes) as resolution increases, statistics are deeply degraded by even small timing and spatial errors.

The resolution increase has a significant impact in reducing NO_2 hourly bias (by 42 %, $2\,\mu g\,m^{-3}$), without any significant change in the error and r (< 2 %). However, O_3 hourly biases increased by less than $1\,\mu g\,m^{-3}$. The main differences between resolutions appear at daytime and nighttime traffic peaks, when the mixing height experiences rapid changes, allowing the 1 km simulation to reduce NO_2 underestimation slightly in the morning by ~ 5–$10\,\mu g\,m^{-3}$. The O_3 daily cycles at large emission sources depict a high influence of hourly NO_2 concentrations, increasing the hourly O_3 bias by $\sim 3\,\mu g\,m^{-3}$. This behavior is controlled by the daytime O_3 underestimation and, to a lesser extent, by the nighttime overestimation. The resolution increase reduces the O_3 overestimations at night by $\sim 5\,\mu g\,m^{-3}$, partly because of higher nocturnal NO_2 concentrations.

Increasing the horizontal resolution improves the model's ability to forecast 75p exceedances in the observed maximum 1 h concentrations. The number of hits that forecast 75p exceedances in the observed Max 1 h NO_2 increases from 466 to 537 over 953 exceedances, while the FAR for Max 1 h O_3 exceedances is reduced by 37 %.

The grid effect is less pronounced for PM_{10} than for NO_2 and O_3. When the resolution increases, the low gradient of PM_{10} mean concentrations ($< 0.1\,\mu g\,m^{-3}$) is the result of compensating for biases of PM_{10} components, which is controlled mainly by the PPM and EC increase, as well as by the SS decrease.

BCN is the domain where the resolution increase has the largest effect, with changes in bias (error) of 16–73 % (< 5 %), followed by AND with 4–43 % (< 5 %) and MAD < 3–5 % (< 1 %). In BCN, as in the western Mediterranean basin, the transport of O_3 and its precursors is governed by mesoscale circulations. In that sense, the resolution increase has a large impact over BCN, where induced mesoscale phenomena control the air flow. Conversely, synoptic transport is more prominent in MAD and AND. Increasing the resolution to 1 km over rural areas (Mass et al., 2002) could contribute to improving the representation of mesoscale meteorological structures such as orographic wind and circulation. Over urban areas along the western Mediterranean coast, further improvements (e.g., models that consider the urban morphology and thermal parameters) are required before seeing any benefits in increasing the resolution to 1 km (Toll and Baldasano, 2002; Jiménez et al., 2006; Fay and Neunhäuserer, 2006).

In urban areas and near large emission sources (industrial and traffic stations), NO_2 and O_3 concentrations are more sensitive to changes in the grid resolution. The concentration increases in primary anthropogenic pollutants (NO_2, PPM and EC), because the high resolution may better allocate emissions at point, linear and area sources. Increased resolution also reduces the artificial dilution of emissions when compared to the larger grid area. Despite the reasons above,

moving to a 1 km horizontal resolution generally did not result in better performance for O_3 and NO_2.

This analysis demonstrates weaknesses in the current model formulations that cannot be resolved with high-resolution modeling only. The subgrid air quality variability at 1-km resolution could not be reproduced over large emissions sources or urban areas, because a finer spatial structure is expected but unresolved. While the work presented here demonstrates the feasibility of modeling on fine scales, there remain many challenges. First, there is a loss of subgrid emissions heterogeneity. Emission inputs to CTM are an average rate, which accounts for the volume-averaged quantity of mass released per unit of time. No other information regarding emissions allocation (e.g., point, linear or per area) is considered; for instance, a large amount of mass can be emitted by a small portion of the grid surface or by several sources scattered around it (Galmarini et al., 2008; Cassiani et al., 2010; Ching and Majeed, 2012). Despite the fact that emissions are estimated by following a bottom-up approach emissions model, emissions heterogeneity is lost in the volume-averaging process performed within CTM. The loss is even higher when resolution decreases (from 1 km to 4 km). Second, there is a low degree of complexity in flow and dispersion details on urban scales, where most of the pollutants come from street canyons and/or tree canopies, and where they are transported until mixing conditions allow the pollutants to disperse above these urban canopy levels (Kim et al., 2013; Ching, 2013). Third, the USGS land-use data used in the WRF model are based on the 1993 data, and urban changes in MAD and BCN over the last 20 years are significant.

Since temperature and wind speed are very sensitive to the ratio of building width to road width, future improvement for fine-scale modeling should focus on using an urban canopy model that considers effects on the transfer of energy and momentum between urban structures and the lower atmosphere. This is crucial for modeling meteorology and air quality on fine scales in urban environments. However, it requires an urban canopy scheme and a canopy parameter database (urban fraction, building height and area). Furthermore, in order to gain any benefits from increasing resolution, the meteorological modeling should be updated to include a better description of land use, instead of relying on USGS data from the year 1993. To this end, the Coordination of Information on the Environment (CORINE) provides a high-resolution (100 m) land-use database, which was developed by the European Environmental Agency and updated to the year 2006 (CLC2006) (EEA, 2007). This could be implemented in the WRF model following the methodology described in Pineda et al. (2004).

Appendix A: Statistical parameters

Table A1. Definition of the discrete statistics used in the evaluation, where $C_m(x, t)$ and $C_o(x, t)$ are the modeled and observed concentrations at a location (x) and time (t); N is the number of pairs of data. $\overline{C_m}$ and $\overline{C_o}$ are the modeled and observed mean concentrations over the whole period, respectively.

Statistic	Formula	
Correlation coefficient	$r = \dfrac{\sum\limits_{i=1}^{N} (C_m(x,t) - \overline{C_m})(C_o(x,t) - \overline{C_o})}{\sqrt{\sum\limits_{i=1}^{N}(C_m(x,t) - \overline{C_m})^2}\sqrt{\sum\limits_{i=1}^{N}(C_o(x,t) - \overline{C_o})^2}}$	(A1)
Mean bias	$MB = \dfrac{1}{N} \sum\limits_{i=1}^{N} (C_m(x,t) - C_o(x,t))$	(A2)
Mean normalized bias error	$MNBE = \dfrac{1}{N} \sum\limits_{i=1}^{N} \dfrac{(C_m(x,t) - C_o(x,t))}{C_o(x,t)} \cdot 100$	(A3)
Mean fractional bias	$MFB = \dfrac{1}{N} \sum\limits_{i=1}^{N} \dfrac{(C_m(x,t) - C_o(x,t))}{(C_o(x,t) + C_m(x,t))/2} \cdot 100$	(A4)
Mean absolute error	$MAE = \dfrac{1}{N} \sum\limits_{i=1}^{N} |C_m(x,t) - C_o(x,t)|$	(A5)
Mean normalized gross error	$MNGE = \dfrac{1}{N} \sum\limits_{i=1}^{N} \dfrac{|C_m(x,t) - C_o(x,t)|}{C_o(x,t)} \cdot 100$	(A6)
Mean fractional error	$MFE = \dfrac{1}{N} \sum\limits_{i=1}^{N} \dfrac{|C_m(x,t) - C_o(x,t)|}{(C_m(x,t) + C_o(x,t))/2} \cdot 100$	(A7)
Root mean squared error	$rmse = \sqrt{\dfrac{1}{N} \sum\limits_{i=1}^{N} (C_m(x,t) - C_o(x,t))^2}$	(A8)

Table A2. Definition of the categorical statistics used in the evaluation. Exceedance analysis is based on a comparison with a fixed threshold concentration (T), where a is the number of false alarms, b is the number of hits, c is the number of correct negatives, and d is the number of misses.

Statistic	Formula	
Accuracy	$A = \left(\dfrac{b+c}{a+b+c+d}\right) \cdot 100$	(A9)
Bias	$B = \left(\dfrac{a+b}{b+d}\right) \cdot 100$	(A10)
Critical success index	$CSI = \left(\dfrac{b}{a+b+d}\right) \cdot 100$	(A11)
Probability of detection	$POD = \left(\dfrac{b}{b+d}\right) \cdot 100$	(A12)
False alarm ratio	$FAR = \left(\dfrac{a}{a+b}\right) \cdot 100$	(A13)

The Supplement related to this article is available online at doi:10.5194/gmd-7-1979-2014-supplement.

References

Appel, K. W., Pouliot, G. A., Simon, H., Sarwar, G., Pye, H. O. T., Napelenok, S. L., Akhtar, F., and Roselle, S. J.: Evaluation of dust and trace metal estimates from the Community Multiscale Air Quality (CMAQ) model version 5.0, Geosci. Model Dev., 6, 883–899, doi:10.5194/gmd-6-883-2013, 2013.

Baldasano, J. M., Cremades, L., and Soriano, C.: Circulation of Air Pollutants over the Barcelona Geographical Area in Summer, in: Proceedings of Sixth European Symposium Physico-Chemical Behaviour of Atmospheric Pollutants, Varese (Italy), 18–22 October, 1993, Report EUR 15609/1 EN, 474–479, 1994.

Baldasano, J. M, Jiménez-Guerrero, P., Jorba, O., Pérez, C., López, E., Güereca, P., Martin, F., García-Vivanco, M., Palomino, I., Querol, X., Pandolfi, M., Sanz, M. J., and Diéguez, J. J.: CALIOPE: An operational air quality forecasting system for the Iberian Peninsula, Balearic Islands and Canary Islands- First annual evaluation and ongoing developments, Adv. Sci. Res., 2, 89–98, 2008.

Baldasano, J. M., Pay, M. T., Jorba, O., Gassó, S., and Jiménez-Guerrero, P.: An annual assessment of air quality with the CALIOPE modeling system over Spain, Sci. Total Environ., 409, 2163–2178, 2011.

Basart, S., Pérez, C., Nickovic, S., Cuevas, E., and Baldasano, J. M.: Development and evaluation of the BSC-DREAM8b dust regional modelo ver Northern Africa, the Mediterranean and the Middle East, Tellus Ser. B, 64, 1–12, 2012.

Byun, D. W. and Schere, K. L.: Review of the governing equations, computational algorithms and other components of the Models-3 Community Multiscale Air Quality (CMAQ) Modeling System, App. Mech. Rev., 59, 51–77, 2006.

Cassiani, M., Vinuesa, J. F., Galmarini, S., and Denby, B.: Stochastic fields method for sub-grid scale emission heterogeneity in mesoscale atmospheric dispersion models, Atmos. Chem. Phys., 10, 267–277, doi:10.5194/acp-10-267-2010, 2010.

Ching, J. K. S.: A perspective on urban canopy layer modeling for weather, climate and air quality applications, Urban Climate, 3, 13–39, 2013.

Ching, J. K. S. and Majeed, M. A.: An approach to characterized within-grid concentration variability in air quality models, Atmos. Environ., 49, 348–360, 2012.

CMAQ: Technical Documentation, available at: http://www.airqualitymodeling.org/cmaqwiki/index.php?title=CMAQversion5. 028February2012release29TechnicalDocumentation, last access: 8 January 2014.

Cohan, D. S., Hu, Y., and Russel, A. G.: Dependence of ozone sensitivity analysis on grid resolution, Atmos. Environ., 40, 126–135, 2006.

Colette, A., Bessagnet, B., Meleux, F., Terrenoire, E., and Rouïl, L.: Frontiers in air quality modelling, Geosci. Model Dev., 7, 203–210, doi:10.5194/gmd-7-203-2014, 2014.

Cuvelier, C., Thunis, P., Karam, D., Schaap, M., Hendriks, C., Kranenburg, R., Fagerli, H., Nyíri, Á., Simpson, D., Wind, P., Schulz, M., Bessagnet, B., Colette, A., Terrenoire, E., Rouïl, L., Stern, R., Graff, A., Baldasano, J. M., and Pay, M. T.: ScaleDep: performance of European chemistry-transport models as function of horizontal spatial resolution, EMEP Report 1/2013, 63 pp., available at: http://emep.int/publ/reports/2013/MSCWtechnical12013.pdf, last access: 4 April 2013.

Eder, B., Kang, D., Mathur, R., Yu, S., and Schere, K.: An operational evaluation of the Eta-CMAQ air quality forecast model, Atmos. Environ., 40, 4894–4905, 2006.

EEA: CLC2006 technical guidelines, EEA Technical Report 17/2007, ISBN 978-90-9167-968-3, doi:10.2800/12134, 70 pp., 2007.

EEA: The application of models under the European Union's Air Quality Directive: A technical reference guide, EEA Technical report 10/2011, Publication Office of the European Union, Luxembourg, ISSN Technical report series 1725-2237, ISBN 978-92-9213-223-1, doi:10.2800/80600, 76 pp., 2011.

EEA: Air quality in Europe – 2013 report, EEA Report 9/2013, ISSN 1725-9177, 112 pp., 2013.

Fay, B. and Neunhäuserer, L.: Evaluation of high-resolution forecasts with the non-hydrostaticnumerical weather prediction model Lokalmodell for urban air pollutionepisodes in Helsinki, Oslo and Valencia, Atmos. Chem. Phys., 6, 2107–2128, doi:10.5194/acp-6-2107-2006, 2006.

Fountoukis, C., Koraj, Dh., Denier van der Gon, H. A. C., Charalampidis, P. E., Pilinis, C., and Pandis, S. N.: Impact of grid resolution on the predicted fine PM by a regional 3-D chemical transport model, Atmos. Environ., 68, 24–32, 2013.

Galmarini, S., Vinuesa, J.-F., and Martilli, A.: Modeling the impact of sub-grid scale emission variability on upper-air concentration, Atmos. Chem. Phys., 8, 141–158, doi:10.5194/acp-8-141-2008, 2008.

Garber, W., Colosio, J., Grittner, S., Larssen, S., Rasse, D., Schneider, J. and Houssiau, M.: Guidance on the Annexes to Decision 97/101/EC on Exchange of Information as revised by Decision 2001/752/EC, Technical Report, European Commission, DG Environment, 2002.

García-Valero, J. A., Montávez, J. P., Jérez, S., Gómez-Navarro, J. J., Lorente-Plazas, R., and Jiménez-Guerrero, P.: A seasonal study of the atmospheric dynamics over the Iberian Peninsula based on circulation types, Theor. Appl. Climatol., 110, 219–310, 2012.

Gego, E., Hogrefe, C., Kallos, G., Voudouri, A., Irwin, J., and Rao, S. T.: Examination of model predictions at different horizontal grid resolutions, Environ. Fluid Mech., 5, 63–85, 2005.

Gonçalves, M., Jiménez-Guerrero, P., and Baldasano, J. M.: Contribution of atmospheric processes affecting the dynamics of air pollution in South-Western Europe during a typical summertime photochemical episode, Atmos. Chem. Phys., 9, 849–864, doi:10.5194/acp-9-849-2009, 2009.

Gong, S. L.: A parameterization of sea-salt aerosol source function for sub- and super-micron particles, J. Geophys. Res., 17, 197, doi:00.1029/2003GB002079, 2003.

Guenther, A., Karl, T., Harley, P., Wiedinmyer, C., Palmer, P. I., and Geron, C.: Estimates of global terrestrial isoprene emissions using MEGAN (Model of Emissions of Gases and Aerosols from Nature), Atmos. Chem. Phys., 6, 3181–3210, doi:10.5194/acp-6-3181-2006, 2006.

Guevara, M., Martínez, F., Arévalo, G., Gassó, S., and Baldasano, J. M.: An improved system for modelling Spanish emissions: HERMESv2.0, Atmos. Environ., 81, 209–221, 2013.

Jiménez, P., Jorba, O., Parra, R., and Baldasano, J. M.: Evaluation of MM5-EMICAT2002-CMAQ performance and sensitivity in complex terrains: High-resolution application to the northeastern Iberian Peninsula, Atmos. Environ., 40, 5056–5072, 2006.

Kain, J. S. and Fritsch, J. M.: A one-dimensional entraining/detraining plume model and its application in convective parameterization, J. Atmos. Sci., 47, 2784–2802, 1990.

Kang, D., Eder, B. K., Stein, A. F., Grell, G. A., Peckham, S. E., and McHenry, J.: The new England air quality forecasting pilot program: development of an evaluation protocol and performance benchmark, J. Air Waste Mange. Assoc., 55, 1782–1796, 2005.

Kim, Y., Sartelet, K., Raut, J.-C., and Chazette, P.: Evaluation of the weather research and forecast/urban model over Greater Paris, Bound.-Lay. Meteorol., 149, 105–132, 2013.

Makar, P. A., Gravel, S., Chirkov, V., Strawbridge, K. B., Froude, F., Arnold, J., and Brook, J.: Heat flux, urban properties, and regional weather, Atmos. Environ., 40, 2750–2766, 2006.

Mass, C., Ovens, D., Albright, M., and Westrick, K.: Does increasing Horizontal resolution Produce better Forecasts? The results of two years of Real-time Numerical Weather prediction in the Pacific Northwest, B. Am. Meteorol. Soc., 83, 407–430, 2002.

Mathur, R., Shankar, U., Hanna, A. F., Odman, M. T., McHenry, J. N., Coats, C. J., Alapaty, K., Xiu, A., Arunachalam, S., Olerud Jr., D. T., Byun, D. W., Schere, K. L., Binkowski, F. S., Ching, J. K. S., Dennis, R. L., Pierce, T. E., Pleim, J. E., Roselle, S. J., and Young, J. O.: Multiscale Air Quality Simulation Platform (MAQSIP): Initial applications and performance for tropospheric ozone and particulate matter, J. Geophys. Res., 110, D13308, doi:10.1029/2004JD004918, 2005.

Millán, M., Salvador, R., Mantilla, E., and Kallos, G.: Photooxidant dynamics in the Mediterranean basin in summer: results from European research projects, J. Geophys. Res., 102, 8811–8823, 1997.

Pay, M. T., Jiménez-Guerrero, P., and Baldasano, J. M.: Implementation of resuspension from paved roads for the improvement of CALIOPE air quality system in Spain, Atmos. Environ., 45, 802–807, 2011.

Pay, M. T., Jiménez-Guerrero, P., Jorba, O., Basart, S., Pandolfi, M., Querol, X., and Baldasano, J. M.: Spatio-temporal variability of levels and speciation of particulate matter across Spain in

the CALIOPE modeling system, Atmos. Environ., 46, 376–396, 2012a.

Pay, M. T., Gassó, S., and Baldasano, J. M.: Evaluation of the CMAQ5.0 in the framework of the CALIOPE air quality forecasting system over Europe, in: 11th Annual CMAS Conference, Chapel Hill, North Carolina, USA, 15–17 October 2012, 2012b.

Pérez, C., Nickovic, S., Baldasano, J. M., Sicard, M., Rocadenbosch, F., and Cachorro, V. E.: A long Saharan dust event over the western mediterranean: Lidar, sun photometer observations, and regional dust modeling, J. Geophys. Res., 111, 1–16, 2006.

Pineda, N., Jorba, O., Jorge, J., and Baldasano, J. M.: Using NOAA AVHRR and SPOT VGT data to estimate surface parameters: application to a mesoscale meteorological model, Int. J. Remote Sens., 25, 129–143, 2004.

Queen, A. and Zhang, Y.: Examining the sensitivity of MM5-CMAQ predictions to explicit microphysics schemes and horizontal grid resolutions, Part III – the impact of horizontal grid resolution, Atmos. Environ., 42, 3869–3881, 2008.

San José, R., Pérez, J. L., Morant, J. L., and González Barras, R. M.: The use of Modern third-generation air quality models (MM5-EMIMO-CMAQ) for real-time operational air quality impact assessment of industrial plants, Water Air Soil Pollu., 9, 27–37, 2009.

Skamarock, W. C. and Klemp, J. B.: A time-split nonhydrostatic atmospheric model for weather research and forecasting applications, J. Comput. Phys., 227, 3465–3485, doi:10.1016/j.jcp.2007.01.037, 2008.

Szopa, S., Foret, G., Menut, L., and Cozic, A.: Impact of large scale circulation on European summer surface ozone and consequences for modelling forecast, Atmos. Environ., 43, 1189–1195, 2009.

Tesche, T. W., Morris, R., Tonnesen, G., McNally, D., Boylan, J., and Brewer, P.: CMAQ/CAMx annual 2002 performance evaluation over the eastern US, Atmos. Environ., 40, 4906–4919, 2006.

Thompson, T. M., Saari, R. K., and Selin, N. E.: Air quality resolution for health impact assessment: influence of regional characteristics, Atmos. Chem. Phys., 14, 969–978, doi:10.5194/acp-14-969-2014, 2014.

Timmermans, R. M. A., Denier van der Gon, H. A. C., Kuenen, J. J. P., Segers, A. J., Honoré, C., Perrussel, O., Builtjes, P. J. H., and Schaap, M.: Quantification of the urban air pollution increment and its dependency on the use of down-scaled and bottom-up city emission inventories, Urban Climate, 6, 44–62, 2013.

Toll, I. and Baldasano, J. M.: Modeling of photochemical air pollution in the Barcelona area with highly disaggregated anthropogenic and biogenic emissions, Atmos. Environ., 34, 3060–3084, 2000.

Valari, M. and Menut, L.: Does an increase in air quality models' resolution bring surface ozone concentrations closer to reality?, J. Atmos. Oceanic Technol., 25, 1955–1968, 2008.

Valverde, V. V., Pay, M. T., and Baldasano, J. M.: Climatic synoptic classification over the Iberian Peninsula oriented to air quality dynamic characterization, Int. J. Climatol., accepted, 2014.

Vivanco, M., Correa, M., Azula, O., Palomino, I., and Martín, F.: Influence of model resolution on ozone predictions over Madrid area (Spain), in: Computational Science and Its Applications–ICCSA 2008, 165–178, Springer Berlin Heidelberg, 2008.

WHO: Review of evidence on health aspects of air pollution – RE-VIHAAP Project Technical report, World Health Organization, Regional Office for Europe, Copenhagen, Denmark, 2013.

Yarwood, G., Roa, S., Yocke, M., and Whitten, G.: Updates to the carbon bond chemical mechanism: CB05, Final report to the US EPA, RT-0400675, 2005.

Zhang, K., Knipping, E., Wexler, A., Bhave, P., and Tonnensen, G.: Size distribution of sea-salt emissions as a function of relative humidity, Atmos. Environ., 39, 3373–3379, 2005.

Zhang, Y., Bocquet, M., Mallet, V., Seigneur, C., and Baklanov, A.: Real-time air quality forecasting, part I: History, techniques, and current status, Atmos. Environ., 60, 632–655, 2012.